

Chapter 12

Inter-spin Interactions of Organic Radical Chains in Organic 1D Nanochannels: An ESR Study of the Molecular Orientations and Dynamics of Guest Radicals



Hirokazu Kobayashi

Abstract Unique inter-spin interaction appears in one-dimensional (1D) organic inclusion compounds which are synthesized by using 2,4,6-tris(4-chlorophenoxy)-1,3,5-triazine (CLPOT) and (*o*-phenylenedioxy) cyclotri phosphazene (TPP). Molecular orientations and dynamics of guest radicals incorporated in CLPOT or TPP nanochannels have been investigated using variable-temperature electron spin resonance (ESR) measurement, together with ESR simulation. When 4-substituted-2,2,6,6-tetramethyl-1-piperidinyloxy (4-X-TEMPO) is incorporated in 1D CLPOT and TPP nanochannels, they exhibited three-dimensional, temperature-independent or 1D, temperature-dependent exchange interactions. It will be possible to design and develop innovative organic magnet based on these features.

Keywords Inclusion compound · 1D nanochannel · Molecular dynamics · Organic magnet · ESR measurement · ESR simulation

12.1 Introduction of Inclusion Compounds

Various new organic functional materials intended for the development of inclusion compounds (ICs) have been developed over the last few decades [1–13]. The guest molecules in ICs occupy nanosized cavities, nanochannels, molecular sheets or jungle-jim-like frameworks in host lattices [12, 14, 15]. The guest compounds within host compounds are mainly governed by van der Waals interaction. Figure 12.1 demonstrates the images of zero- to three-dimensional nanopspaces and the included guest molecules. The nanopspaces within the host materials are called as one-dimensional (1D) when their structures are tunnel-like cavities,

H. Kobayashi (✉)

Faculty of Arts and Sciences at Fujiyoshida, Showa University, Yamanashi, Japan
e-mail: hirawk@cas.showa-u.ac.jp

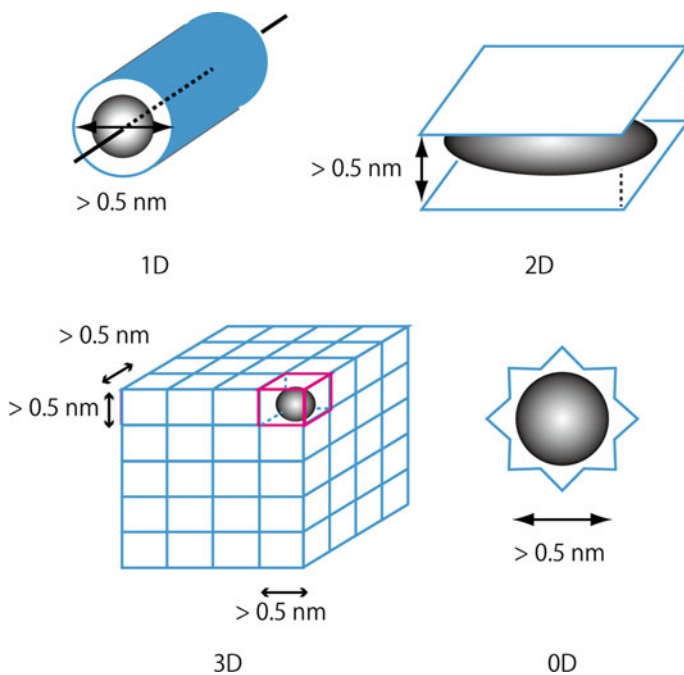
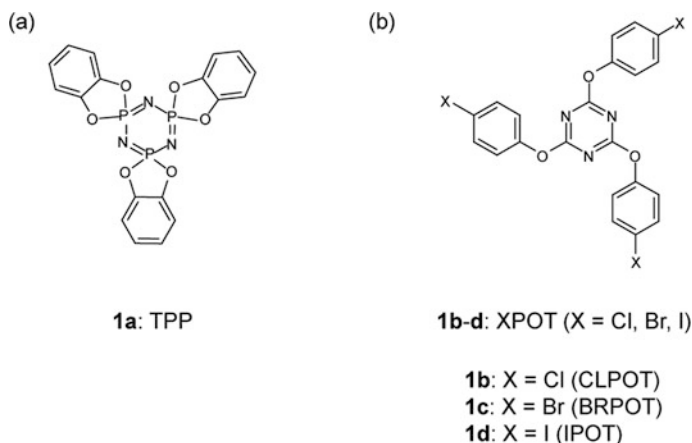


Fig. 12.1 Images of 0–3D nanospaces and the included guest molecules. Black-and-white spherical objects demonstrate guest materials

two-dimensional (2D) in the case sandwiched between molecular sheets, and three-dimensional (3D) in the case stacked jungle-jim-like. On the other hand, when guest molecules are included in the center of circular host molecules, such as crown ether, cyclodextrin, or micelles, they are called as zero-dimensional (0D) for convenience[16]. In 1–3D host materials, when the pores of host materials are kept even in the guest desorption by heating or pH change such as zeolite, they are called as *porous materials*. Many researchers have employed 0–3D host materials with periodic and regular cavities, including 1D nanochannels serving as nanosized molecular templates to align guest molecules [11–13, 17–19]. ICs such as these are expected to exhibit anisotropic physical properties. As an example, the 1D alignment of paramagnetic molecules in 1D nanochannel may generate the array of dimers, trimers, or multi-metric assembly of electron spins and may give rise to anisotropic magnetic characteristics by the intra- or interchain magnetic interactions. Such materials have attracted attention with regard to the fabrication of novel molecular-scale magnets and electric devices [11–13, 17–24] and medications based on magnetic markers [25] and also have applications in magnetic resonance spectroscopy [26, 27].

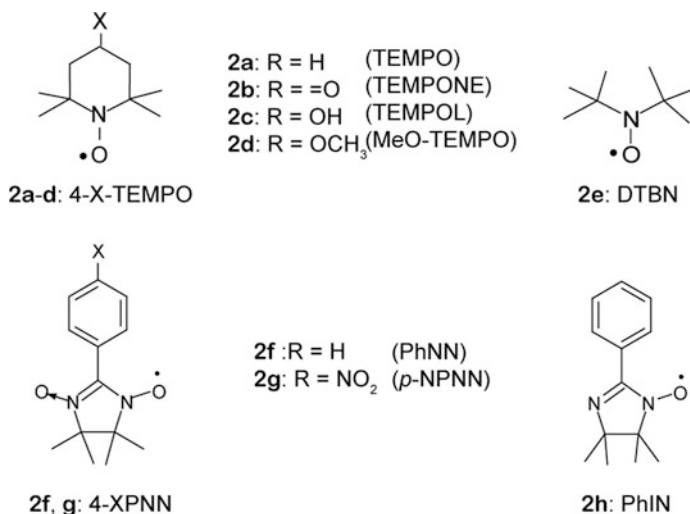
Crystalline tris(*o*-phenylenedioxy)cyclotriphosphazene (TPP: Scheme 12.1a) has tunnel-like 1D nanochannels in which the walls comprise locally trigonally coordi-



Scheme 12.1 Chemical structures of host compounds described in this review: TPP (a) and XPOT (b–d)

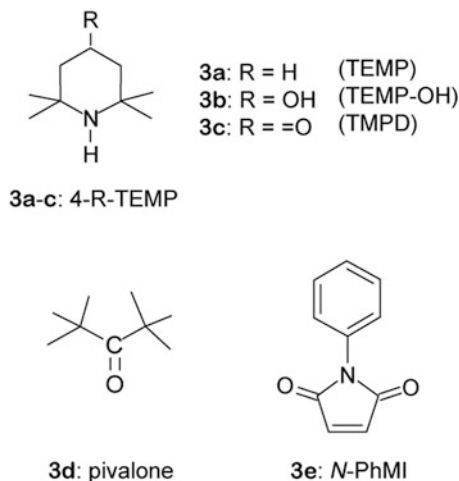
nated phenyl rings [14, 28]. The pore size of these nanochannels, 0.45 nm in the guest-free state [29], can be expanded to 0.9 nm by including guest molecules. The homogeneity of TPP nanochannels has been examined using hyperpolarized and high-pressure ^{129}Xe nuclear magnetic resonance (NMR) spectroscopy [30–32]. During the recrystallization of TPP, solutes within the solvent and the solvent molecules themselves can be included in TPP nanochannels in a 1D manner to form molecular chains. The extent of inclusion in these nanochannels is decided by the molecular size and the concentration of the guest molecules. If functional molecules having unique electrical characteristics are included in the TPP nanochannels, the resulting ICs may express anisotropic optical, electric, or magnetic properties. As an example, TPP ICs including dye molecules exhibit an anisotropic second harmonic generation effect due to the charge transfer direction in the guest molecules [33, 34] and those including I_2 exhibit anisotropic electron conductivity parallel or perpendicular to the channel axes due to electron donor properties of guest atoms or molecules and the dielectric host structures which separates I_2 chains [35].

TPP-based ICs incorporating sulfur-nitrogen or alkyl stearate radical molecular chains have been assessed by several groups [36, 37]. The formation of 1D molecular chains of 2,2,6,6-tetramethyl-1-piperidinyloxy (TEMPO; Scheme 12.2a) radicals was achieved using the 1D nanochannels of TPP crystals ($[(\text{TPP})_2(\text{TEMPO})_{1.0}]$; **1a/2a**) [38, 39]. Electron spin resonance (ESR) analyses of **1a/2a** demonstrated isotropic line profiles over all temperature range, in particular intermediate between Lorentzian and Gaussian above 139 K. In addition, a narrowing of the peak-to-peak line width was associated with the 1D spin diffusion behavior in this material ($|J_{\text{intra}}| < 1$ K) (see Sects. 12.2.5 and 12.6). On the other hand, the inclusion amount of the guest radicals in nanochannels can be reduced using non-radical molecules such as 2,2,6,6-tetramethylpiperidine (TEMP; Scheme 12.3a), which are similarly sized to the guest radicals. Then, the ICs demonstrate high-



Scheme 12.2 Chemical structures of guest radicals described in this review: 4-substituted-TEMPO derivatives (4-X-TEMPO: **a–d**), DTBN (**e**), 4-substitute-PhNN (4-XPNN: **f** and **g**), and PhIN (**h**)

Scheme 12.3 Chemical structures of spacers described in this review: 4-substituted-TEMP derivatives (4-R-TEMP: **a–c**), pivalone (**d**), and *N*-PhMI (**e**)



resolved ESR spectra due to the reduction of dipolar broadening. Above 108 K, TEMPO radicals dispersed in TPP nanochannels by TEMP were found to undergo anisotropic rotational diffusion around the principal *y*-axis of the *g* tensors of the radicals, which were perpendicular to the molecular long axis (see Sects. 12.2.3 and 12.5) [40]. These results suggest the possibility of correlating the inter-spin exchange/dipolar interactions of **1a/2a** with the molecular dynamics of TEMPO radicals in TPP nanochannels. **1a/2a** undergo antiferromagnetic exchange interactions at quite low temperatures, indicating that one-dimensional organic

Table 12.1 Host, guest, and spacer described in this chapter

	Roles	Materials	Example
Host	Nanochannel	1–3D porous material	TPP, XPOT
Guest	Magnetic source	Organic radical	4-X-TEMPO (including DTBN), 4-XPNN, PhIN
Spacers	Reduction of guest inclusion in nanochannel	Non-radical molecule	4-R-TEMP, pivalone, <i>N</i> -PhMI

inclusion compounds incorporating organic radical (1D OIC-OR) may potentially be synthesized from these compounds. Such materials could be used to probe the magnetic exchange between radicals, based on the appropriate selection of host and guest materials so as to tune the molecular orientations and dynamics of the guest radicals in the nanochannels. In the case of several TPP ICs incorporating organic radicals such as **2a–c** (**2b**: 4-oxo-TEMPO (TEMPONE), **2c**: 4-hydroxy-TEMPO (TEMPOL)), **e** (di-*t*-butyl nitroxide (DTBN)), **f** (phenylnitronyl nitroxide (PhNN)), and **h** (phenyl iminonitroxide (PhIN)), the molecular orientation and dynamics of guest molecules in nanochannels have been determined using ESR spectroscopy [41–44] as well as theoretical simulation of spectra [45–47] (see Sects. 12.2.3 and 12.5). These techniques can be employed to determine the molecular orientations and dynamics of organic radicals both in 1D nanochannels and 0D cavities [48, 49]. In Table 12.1, the characters of host, guest, and spacer materials described in this review are summarized.

In other work, the 1D nanochannels of 2,4,6-tris(4-chlorophenoxy)-1,3,5-triazine (CLPOT: Scheme 12.1b) [50] crystals have been used to confine several organic radicals, including 4-substituted-TEMPO derivatives (4-X-TEMPO: Schemes 12.2a–d) [51, 52] and 4-substituted-phenylnitronyl nitroxides (4-XPNN: Schemes 12.2f and g) [27]. The 1D rotational diffusion of these radicals in CLPOT nanochannels has been confirmed, based on the ESR spectra of radicals in the nanochannels and numerical simulations (see Sects. 12.2.3 and 12.4). CLPOT ICs incorporating 1D 4-X-TEMPO molecular chains have demonstrated temperature-independent 3D exchange interactions and exchange narrowing in the temperature range from 4.2 to 300 K (see Sect. 12.6) [53]. These results indicate, as predicted, the proper choice of host materials, and guest radicals can control the inter-spin interaction in 1D OIC-OR.

In the synthesis of 1D OIC-OR, CLPOT crystals are preferable to TPP as a host material, as these crystals allow the inclusion of many different types of organic radicals. This is due to the pore diameters in the former, which are comparable to the molecular cross section of many stable nitroxide or NN (nitronyl nitroxide) radicals (*ca.* 1.1–1.3 nm in CLPOT but 0.45–0.9 nm in TPP) as well as the suitable polarity of the former (as radicals frequently have polar substituent groups). However, it is possible to include several types of guest radicals in TPP nanochannels by following the appropriate stepwise process [41, 44]. Prior work concerning the determination of the molecular orientations and dynamics of NN or IN (iminonitroxide) radicals in TPP or CLPOT nanochannels using ESR has demonstrated the feasibility of

developing a new ESR spin probe technique based on NN groups [27, 44]. For the reasons described above, 1D OIC-OR represent an important new type of magnetic material.

Both organic porous materials and metal organic frameworks [11, 13] can be used as molecular templates for the array of guest radicals. In addition, 0D, 2D, or 3D porous materials may be employed to produce magnetic inclusion compounds instead of those having 1D nanochannels. As an example, 2,4,6-tris(4-bromophenoxy)-1,3,5-triazine (BRPOT: Scheme 12.1c) [50], one possible derivative of 2,4,6-tris(4-halophenoxy)-1,3,5-triazine (XPOT: Scheme 12.1b–d), can contain several different guest molecules, including Buckminsterfullerenes [54–56]. However, the cavities of XPOT derivatives other than CLPOT do not necessarily have 1D structures. These difference in morphology originate from the inter-atom interactions between halogen atoms in the XPOT crystals [50].

In this review, the molecular orientations and dynamics of various guest radicals, as an example, 4-X-TEMPO, 4-XPNN, or PhIN, in CLPOT or TPP 1D nanochannels are described based on the ESR analyses. In addition, the inter-spin interactions of 4-X-TEMPO radical chains formed in the CLPOT or TPP nanochannels are explained in relation to the molecular dynamics of 4-X-TEMPO in the nanochannels. In Sect. 12.2, theoretical background of ESR and the calculation method in ESR simulation using EasySpin program [46, 47] are introduced. Sample preparation and characterization of 1D OIC-OR are noted in Sect. 12.3. The molecular dynamics of guest radicals in CLPOT- or TPP-based 1D OIC-ORs are explained in Sects. 12.4 and 12.5, respectively. Remarkable exchange interaction in CLPOT- or TPP-based 1D OIC-ORs with 4-X-TEMPO chains are explained in Sect. 12.6. Finally, in Sect. 12.7, the conclusion and outlooks in the future of this study are described.

12.2 Theoretical Background and ESR Simulation

12.2.1 *Electron Spin Resonance*

In ICs, magnetic resonance spectroscopy is a powerful means of elucidating the molecular structures of host materials and the molecular orientations and the dynamics of guest radicals in host nanochannels, in addition to assessing inter-spin interactions and magnetism of guest radical chains. When the researchers tune into the unpaired electrons in guest radicals or the electric properties of 1D OIC-ORs (as examples, conductivity, dielectric or magnetism), they may use electron spin resonance (ESR) spectroscopy, whereas nuclear magnetic resonance (NMR) spectroscopy is available for the study when they are interested in the molecular structures or the dynamics of non-radical compounds. The reader is referred to several texts that provide detailed discussions of magnetic resonance spectroscopy [57–60].

When a sample with unpaired electrons is inserted into an external magnetic field \mathbf{B}_0 , the magnetic moments of electrons in the material are split into different energy levels, depending on whether these moments are parallel or antiparallel to \mathbf{B}_0 . The electron magnetic moment operators are proportional to the electron spin angular momentum values, and the proportionality constant γ (also referred to as the gyromagnetic ratio) will be negative for electrons. Therefore, the electron magnetic moment will be antiparallel to the angular momentum. In the external magnetic field, the electron spin magnetic moments precess around \mathbf{B}_0 at the Larmor frequency ω_0 , which equals $-\gamma\mathbf{B}_0$. The Larmor frequencies of the various electron magnetic moments in a specimen will differ according to the shielding effect of neighboring electrons and/or nuclei. If an electromagnetic wave whose frequency corresponds to the energy difference of the magnetic moments in the field, ($\Delta E = h\nu = \hbar\omega = \gamma\hbar B$) is applied to the sample, the electron spins in the ground states will be excited. This phenomenon is the basis of ESR, which focusses on electron spins. ESR studies employ a magnetic field (generated using an electric magnet) that sweeps over the range of 0–1 T in conjunction with continuous-wave (cw) microwave irradiation (1–100 GHz) of a sample in a cavity resonator. Pulse ESR methods are also used for the clarification of complicated spin-lattice or inter-spin interactions. Variable-temperature ESR over the temperature range from 4.2 to 400 K can be applied to determine the spin concentration of each IC, as well as the molecular orientations and dynamics of organic radicals in 1D nanochannels and the inter-spin interactions and magnetism of 1D organic radical chains constructed in the 1D nanochannels. In this review, the theoretical background of the analysis of free radicals in 1D nanochannels by ESR spectroscopy is described in detail.

12.2.2 Nuclear Magnetic Resonance

When a sample without unpaired electrons is used, electron spins in the description in the prior subsection can be replaced into nuclear magnetic moments (more properly, only in the case of $I = 1/2$ (I : the nuclear spin quantum number of the nuclei)). If $I > 1/2$, see Sect. 12.2.3.1 and references [57–59]). However, the proportionality constant γ will be positive for most nuclei. Therefore, the nuclear magnetic moment will typically be parallel to the angular momentum. In modern-day NMR analyses, radio-frequency pulses (ω ; in the range of 10^2 – 10^3 MHz) are applied to a sample surrounded by a coil and subjected to an external magnetic field of approximately 1–15 T in conjunction with a superconducting magnet. In the case of metals or metal nanoparticles, analyses are conducted in a static external magnetic field using a cw radio-frequency source with either a permanent or electric magnet [60, 61]. Room temperature solution ^1H NMR spectroscopy is primarily performed for the structural elucidation of host materials such as TPP and CLPOT.

12.2.3 ESR Simulation

12.2.3.1 g Tensor and A Tensor

The ESR spectra for the free radicals in 1D nanochannels is reproducible using EasySpin program for the ESR spectral reproduction under various conditions of electron and nuclear spins [62]. The total spin Hamiltonian used in EasySpin is as follows:

$$\hat{H} = \sum_i \left(\hat{H}_{\text{EZI}}(i) + \hat{H}_{\text{ZFI}}(i) \right) + \sum_i \left(\hat{H}_{\text{NZI}}(k) + \hat{H}_{\text{NQI}}(k) \right) + \sum_i \sum_{j>i} \hat{H}_{\text{EEI}}(i, j) + \sum_i \sum_k \hat{H}_{\text{HFI}}(i, k) \quad (12.1)$$

with the following terms: $\hat{H}_{\text{EZI}}(i)$, electron-Zeeman interaction (EZI) between electron spin i with an external magnetic field; $\hat{H}_{\text{ZFI}}(i)$, zero-field interaction (ZFI) of electron spin i with adjacent electron spins in the case of $S > 1/2$ (S , the total spin quantum number of electrons in the system); $\hat{H}_{\text{NZI}}(i)$, nuclear-Zeeman interaction (NZI) between nuclear spin k with an external field; $\hat{H}_{\text{NQI}}(i)$, nuclear quadrupole interaction (NQI) between nuclear spin k with $I > 1/2$ (I , the nuclear spin quantum number of the nuclei) having an electric quadrupole moment that can interact with the local electric field gradient at the nucleus; $\hat{H}_{\text{EEI}}(i, i)$, electron-electron interaction (EEI) between electron spin i and j as an example, exchange interaction; and $\hat{H}_{\text{HFI}}(i, k)$, hyperfine interaction (HFI) between electron spin i and nuclear spin k at the nucleus. In this review, $\hat{H}_{\text{NZI}}(i)$ and $\hat{H}_{\text{NQI}}(i)$ are ignored due to the small influence in the electron spin system and also $\hat{H}_{\text{ZFI}}(i)$ and $\hat{H}_{\text{EEI}}(i, i)$ due to the quite isolated spin system without zero-field splitting or exchange interaction.

Therefore, the spin Hamiltonian for the free radicals isolated in 1D nanochannels, as examples, 4-X-TEMPO (**2a–e**), 4-XPNN (**2f** and **g**), and PhIN (**2h**), is simplified as follows:

$$\hat{H} = \beta_e \mathbf{B} \cdot \mathbf{g} \cdot \hat{S} + \hat{S} \cdot \sum_{p=1,2} A_p \cdot \hat{I}_p + \beta_n g_n \mathbf{B} \cdot \sum_{p=1,2} A_p \cdot \hat{I}_p \quad (12.2)$$

where β_e , \mathbf{B} , \mathbf{g} , A_p , β_n , g_n , \hat{S} , and \hat{I}_p are the Bohr magneton, the laboratory magnetic flux density vector (corresponding to the external magnetic field), the electron spin g tensor, the hyperfine tensor for the p th ^{14}N nucleus, the nuclear magneton, the nuclear spin g -factor, the electron spin operator, and the nuclear spin operator for the p th ^{14}N nucleus in the radicals, respectively [27, 41–44, 51, 52, 63, 64]. \mathbf{g} and A_p are described as diagonal matrices

$$\mathbf{g} = \begin{pmatrix} g_{xx} & 0 & 0 \\ 0 & g_{yy} & 0 \\ 0 & 0 & g_{zz} \end{pmatrix} \quad (12.3)$$

$$\mathbf{A}_p = \begin{pmatrix} A_{pxx} & 0 & 0 \\ 0 & A_{pyy} & 0 \\ 0 & 0 & A_{pzz} \end{pmatrix} \quad (12.4)$$

via a rotation matrix parameterized by three Euler angle where g_{qq} and A_{qq} ($q = x, y, z$) are the three principal values of the \mathbf{g} and \mathbf{A}_p matrices [62]. If $p = 1$, the summation sign in Eq. (12.2) may be often omitted for simplification. The isotropic components of \mathbf{g} and \mathbf{A}_p are defined by $g_{\text{iso}} = (g_{xx} + g_{yy} + g_{zz})/3$, and $(A_p)_{\text{iso}} = (A_{pxx} + A_{pyy} + A_{pzz})/3$.

In the case of 4-X-TEMPO, the single nitrogen atom of the nitroxide (NO) group is considered (i.e., $p = 1$), whereas the nitrogen atoms of the nitronyl and/or imino nitroxide groups (i.e., $p = 1$ or 2) in 4-XPNN and PhIN radicals are considered.

The principal axes of the 4-X-TEMPO radicals are defined such that the z -axis is perpendicular to the NO group, and along the $2p_z$ orbital of the NO group, the x -axis is parallel to the NO bond and the y -axis is perpendicular to the zx plane [65]. The principal axes of the \mathbf{g} and \mathbf{A} tensors are coincident. The \mathbf{A} tensor of the NO radicals is quite anisotropic, such that $A_{zz} > A_{xx}, A_{yy}$ [51, 52, 63–65]. To ensure accurate reproduction of the ESR spectra, the A_{xx} and A_{yy} values for 4-X-TEMPO are assumed to be similar, while cylindrical symmetry of the \mathbf{A} tensor is not necessarily assumed.

The principal axes of the 4-XPNN radicals are defined such that the z -axis is perpendicular to the molecular plane of the NN group of 4-XPNN, the y -axis is parallel to the bond between the NN group and phenyl ring, and the x -axis is perpendicular to the yz plane [27, 44, 66]. Therefore, the \mathbf{g} tensor for the 4-XPNN radical is determined as follows [66]. The unpaired electron of the NN group is associated with a π orbital. As such, the lowest component of the \mathbf{g} tensor should be observed perpendicular to the molecular plane of the NN group (i.e., the principal z -axis direction) and should have a value of approximately 2.0023. In molecular orbital calculations, $g_{xx} > g_{yy} > g_{zz}$ for the 4-XPNN radical (i.e., the intensity of the g_{xx} component is observed at the leftmost (lowest magnetic field) side). With respect to the \mathbf{A} tensor for the 4-XPNN radical, the unpaired electron occupies the π orbital composed of the $2p_z$ orbitals of the nitrogen atoms (having considerable spin density), such that A_{zz} is major component, with A_{xx} and A_{yy} being minor components. Therefore, the \mathbf{A} tensor for NN radicals is also quite anisotropic. Although the local axes of the \mathbf{A} tensors of the two nitrogen nuclei of the 4-XPNN radical are expected to be different, it is assumed that the unpaired electron interacts with the two nitrogen nuclei with an averaged \mathbf{A} tensor, so as to simplify the analysis. In this approximation, the principal axes of the \mathbf{g} and \mathbf{A} tensors for the 4-XPNN radical will be coincident.

The principal axes of the g tensor of the PhIN radical are assumed to be similar to those of the 4-XPNN radical and also consistent with NN due to the higher spin density on the NO group [44]. However, it should be noted that $A_1 \neq A_2$ for IN radicals ($(A_1)_{\text{iso}} > (A_2)_{\text{iso}}$), [44, 67] where A_1 is the hyperfine tensor of the NO nitrogen of the IN groups and A_2 is that of the 3-position nitrogen. Since the xx and yy components of A_1 and A_2 are much smaller than the zz component, the principal axes of the g , A_1 , and A_2 tensors for the IN radicals are also assumed to be coincident to allow for simplified calculations, similar to the procedure for 4-XPNN radicals.

12.2.3.2 Calculation Procedure

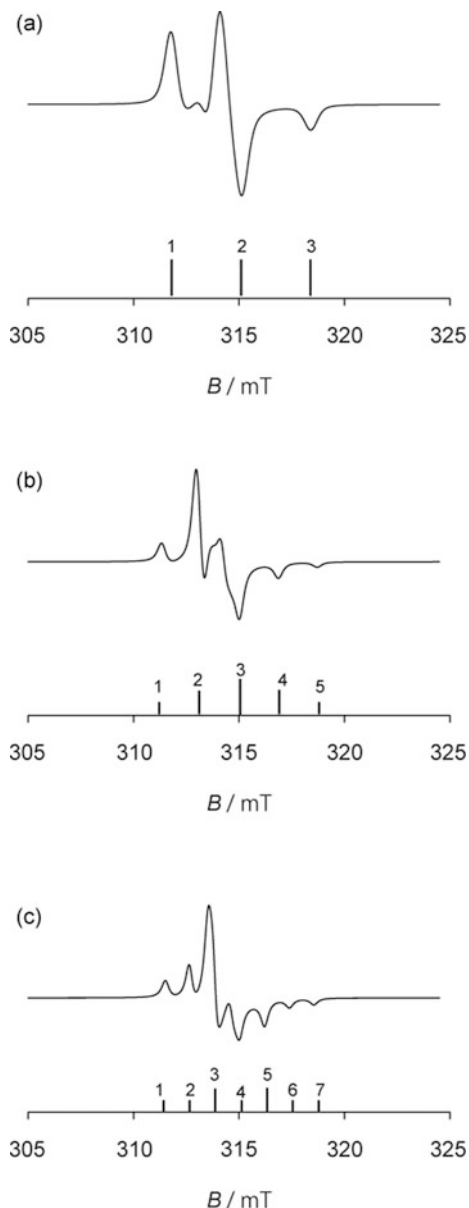
To determine the molecular orientations and dynamics of guest radicals in 1D nanochannels, the ESR spectra of isolated radicals must be reproduced in detail, because these spectra provide information concerning the principal values of the g and A tensors. Such spectra can be generated based on theoretical calculations. EasySpin program is a component of the MATLAB software package (MathWorks, Natick, MA, USA), developed by Stoll and intended for the simulation and fitting of a wide range of ESR spectra (EasySpin 5.2.20, ETH Zürich) [46, 47]. EasySpin program provides extensive ESR-related functionality, ranging from spin physics to data analysis. This software also contains routines for the simulation of liquid- and solid-state ESR and electron-nuclear double resonance data. The programming language of MATLAB is based on matrices and very efficient matrix algorithms, and EasySpin program consists of over 80 MATLAB functions that perform a variety of ESR-related tasks. Functions from the larger and more basic category provide the core functionality necessary for computational ESR. Building on this foundation, a small number of general, robust high-level functions for spectral simulation are provided.

This sub-subsection references a number of programs. These include the Pepper, which is used to produce the field-swept and frequency-swept solid-state cw ESR spectra of powders and crystals; Chili, which simulates field- and frequency-swept cw ESR spectra in the slow-motion regime on the ESR time scale; and Garlic, which produces the isotropic or anisotropic fast-motion cw ESR spectra of radicals in solution or nanospaces. Calculations for 4-XPNN and PhIN radicals with two ^{14}N atoms ($I = 1$) based on the interactions of electron spins can be performed using a PC with more than 8 GB of RAM. Chili requires more memory to generate spectral reproductions for 4-XPNN or PhIN radicals, and so the allocation function of Opt within the program parameters, as an example, should be set to `Opt.Allocation = [4e7 2e5]` [47].

12.2.3.3 Rigid-Limit ESR Spectra

Figure 12.2 presents typical rigid-limit ESR spectra for nitroxide, NN, and IN radicals as simulated using the EasySpin Pepper program to calculate solid-state

Fig. 12.2 Typical rigid-limit ESR spectra for powder (a) nitroxide [52] (b) NN [27] and (c) IN radicals [44] using the EasySpin Pepper program [46, 47]. Bars on the horizontal axis in each figure indicate the major hyperfine coupling interactions by equivalent or inequivalent nitrogen atoms



cw spectra. In Fig. 12.2a–c, the three, five, or seven major hyperfine interaction lines associated with the equivalent/inequivalent nitrogen atoms having unpaired electrons in the substituent groups are shown on the horizontal axis for convenience. These spectra were reproduced using the principal values of the g and A tensors of unpaired electrons, along with line width parameters and signal amplitudes. The g

Table 12.2 Tensor components of the g , A_p , and line width parameters (G, Gaussian component; L, Lorentzian component) for the reproduced ESR spectra of nitroxide, NN, and IN radicals presented in Fig. 12.2

State of radicals	g_{xx}	g_{yy}	g_{zz}	$A_{1xx}(/A_{2xx})/mT$	$A_{1yy}(/A_{2yy})/mT$	$A_{1zz}(/A_{2zz})/mT$	Line width	
							G/mT	L/mT
Fig. 12.2a (nitroxide radicals) ^a	2.0095	2.0066	2.0023	0.06	0.06	3.30	0.50	0.40
Fig. 12.2b (NN radicals) ^b	2.0120	2.0075	2.0028	0.02	0.03	1.84	0.20	0.40
Fig. 12.2c (IN radical) ^c	2.0103	2.0050	2.0028	0.01 0.02	0.01 0.02	2.36 1.16	0.10	0.40

^aRef. [52]. ^bRef. [27]. ^cRef. [44]

and A tensors for each radical were estimated from experimental data by setting default values for g_{zz} and A_{zz} based on the hyperfine coupling lines associated with isolated radicals acquired at both ends of low-temperature ESR spectra, assuming that the molecular motion of the radicals was frozen. The values of g_{xx} and g_{yy} and of A_{xx} and A_{yy} are difficult to determine directly from ESR spectra, and so these were initially estimated by visual inspection of the simulations of ESR spectra generated using EasySpin program. The final values for each component of the g and A tensors of each radical were estimated via the step-by-step variation of these components or g_{qq} and A_{qq} ($q = x, y$ or z) along with the line width parameters and signal amplitudes, so as to minimize the sum of the squares of the difference between the experimental and simulated spectra. The number of the A tensor in Eq. (12.2) will vary according to the number of equivalent/inequivalent nitrogen atoms in substituent groups on which unpaired electron is localized. The principal axis components of the g and A tensors for the reproduced ESR spectra shown in Fig. 12.2 are summarized in Table 12.2.

The EasySpin program expresses the line shape using a Voigt function based on the Gaussian broadening (convolution) of a Lorentzian line [46, 47, 68]. In the present analysis, the full width at half maximum (FWHM) is employed as the line width parameter, and the Gaussian and Lorentzian line width components for the reproduced ESR spectra shown in Fig. 12.2 are also provided in Table 12.2.

The three major hyperfine interaction lines associated with the nitrogen atoms in the NO groups of nitroxide radicals are shown on the horizontal axis in Fig. 12.2a for convenience. These supplementary lines have equivalent peak heights when the ESR spectrum is acquired in dilute solution. In the case of the reproduction of an NN radical spectrum in Fig. 12.2b, the five major hyperfine interaction lines associated with equivalent nitrogen atoms having the same hyperfine coupling constants are included on the horizontal axis. The peak heights of these supplementary lines are proportional to their peak intensities in dilute solution, (i.e., 1:2:3:2:1). Although lines 1, 2, 4, and 5 are well-resolved, the shape of line 3 is more complicated

Table 12.3 Tensor components of the g and A tensors for various organic radicals in the various states. Spacer molecules are abbreviated in each state

State of radicals	g_{xx}	g_{yy}	g_{zz}	$A_{1xx}/(A_{2xx})/mT$	$A_{1yy}/(A_{2yy})/mT$	$A_{1zz}/(A_{2zz})/mT$
TEMPO in TPP ^a	2.0100	2.0070	2.0024	0.60	0.55	3.35
DTBN in TMCB ^b	2.0088	2.0062	2.0027	0.76	0.60	3.18
DTBN in TPP ^c	2.0090	2.0062	2.0022	0.50	0.50	3.48
TEMPOL in TPP ^d	2.0092	2.0061	2.0026	0.83	0.30	3.33
TEMPO in CLPOT ^e	2.0102	2.0062	2.0023	0.73	0.60	3.35
MeO-TEMPO in CLPOT ^f	2.0098	2.0062	2.0024	0.56	0.43	3.43
PhNN in rigid Duco Cement ^g	2.0127	2.0068	2.0028	0.52	0.52	1.80
PhNN in CLPOT ^h	2.0118	2.0075	2.0031	0.34	0.12	1.74
PhNN in TPP ⁱ	2.0107	2.0086	2.0031	0.01	0.01	2.13
<i>p</i> -NPNN in CLPOT ^h	2.0116	2.0076	2.0030	0.32	0.16	1.77
PhIN glassy toluene ^j	2.00932	2.00604	2.00222	–	–	2.32/1.28
PhIN in TPP ⁱ	2.0103	2.0050	2.0028	0.02/0.01	0.01/0.02	2.36/1.16

TMBC tetramethyl-1,3-cyclobutanedione

^aRef. [40]. ^bRef. [64]. ^cRef. [41]. ^dRef. [43]. ^eRef. [51]. ^fRef. [52]. ^gRef. [66]. ^hRef. [27]. ⁱRef. [44]. ^jRef. [67]

[66]. This occurs because the g_{xx} and g_{yy} components are larger than the g_{zz} component and because the A_{xx}^{NN} and A_{yy}^{NN} components are much smaller than the A_{1zz}^{NN} component. In the case of PhIN results in Fig. 12.2c, the seven major hyperfine interaction lines associated with inequivalent nitrogen atoms having different hyperfine coupling constants (typically, $A_{1zz}^{IN} \sim 2A_{2zz}^{IN}$) are included. The peak heights of these lines are proportional to the peak intensities obtained from analyses in dilute solution. Here, lines 1, 2, 5, 6, and 7 are well-resolved, and the spectrum between lines 3 and 4 is more complicated [44]. These results are due to the g_{xx} and g_{yy} components, which are large relative to the g_{zz} components, and to the A_{1xx}^{IN} , A_{1yy}^{IN} , A_{2xx}^{IN} , and A_{2yy}^{IN} components, all of which are much smaller than the A_{1zz}^{IN} or A_{2zz}^{IN} components. The principal axis components of the g and A tensors of several organic radicals in various states are provided in Table 12.3.

12.2.3.4 Anisotropic Rotational Diffusion

When simulating ESR spectra at higher temperatures (at which the molecular motions of radicals in the 1D nanochannels are increased), it is assumed that the rotational axis of each organic radical can be defined by polar and azimuthal angles, θ and ϕ , respectively, in the principal axis system of the g tensor for each radical [27]. As noted, the Chili program within the EasySpin package allows ESR spectra in the slow-motion regime to be generated [46, 47]. These simulations are based on solving the stochastic Liouville equation on the basis of rotational eigenfunctions.

In the case of a molecule that undergoes numerous collisions that cause small random angular reorientations, the resultant anisotropic rotational motion is a Markov process [45]. If Ω is defined as the Euler angle for a tumbling molecular axis with respect to a fixed laboratory axis system, the probability of finding the molecule in direction Ω at time t is defined as $P(\Omega, t)$. In a Markov process, the probability of being in state Ω_1 at time t , if in state Ω_2 at time $t - \Delta t$, is both independent of the Ω value at any time earlier than $t - \Delta t$ and dependent only on Δt rather than t . As such, $P(\Omega, t)$ can be described by the rotational diffusion equation:

$$\frac{\partial P(\Omega, t)}{\partial t} = R \nabla_{\Omega}^2 P(\Omega, t) \quad (12.5)$$

where ∇_{Ω}^2 is the Laplacian operator on the surface of a unit sphere and R is the rotational diffusion coefficient. If the molecule is approximated by a rigid sphere of radius a rotating in a medium of viscosity η , the rotational Stokes-Einstein relationship yields

$$R = \frac{kT}{8\pi a^3 \eta} \quad (12.6)$$

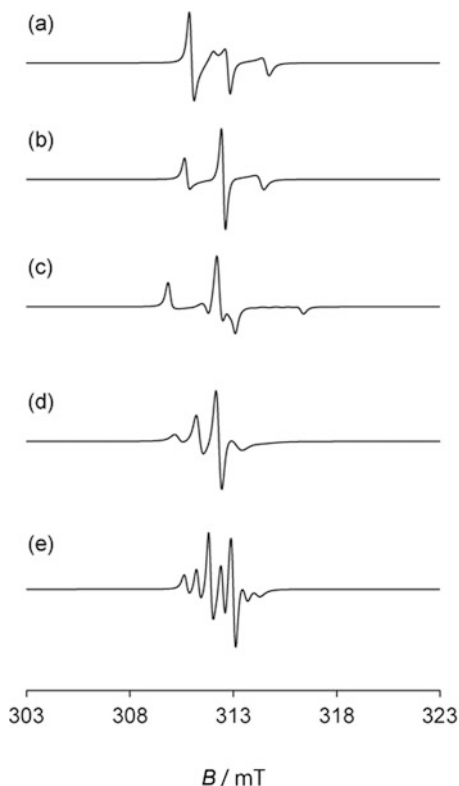
In an anisotropic liquid, the average rotational diffusion correlation time τ_R is given by:

$$\tau_R = \left(6\sqrt{R_{\parallel}R_{\perp}}\right)^{-1} \quad (12.7)$$

where R_{\parallel} and R_{\perp} are defined as the parallel and perpendicular components of R . It is expected that Eqs. (12.5, 12.6, and 12.7) can be applied to anisotropic molecular rotational diffusion in organic 1D nanochannels [27, 44, 51, 52]. Thus, in ESR simulations, highly anisotropic R_{\parallel} and R_{\perp} components, such as $R_{\parallel}/R_{\perp} \approx 1000$, are assumed.

The θ and ϕ values for nitroxide, NN, and IN radicals can be estimated by varying τ_R along with the line width parameters and signal amplitudes so as to obtain the best fit to the ESR spectrum at the highest temperature. At elevated temperatures, the molecular motions of guest radicals in the 1D nanochannels will be in the slow-motion regime (10^{-6} s $>$ τ_R $>$ 10^{-9} s) on the ESR time scale. Using these θ

Fig. 12.3 Simulated ESR spectra of nitroxide, NN, and IN radicals, modulated on the basis of anisotropic rotational diffusion around the principal x , y , and z axes of the g tensor (a–c), the principal y -axis of the g tensor (d), and (again) the principal y -axis of the g tensor (e), respectively, using the Chili program within the slow-motion regime with respect to the ESR time scale [27, 41, 44, 52]



and ϕ values, τ_R is similarly estimated at additional temperatures by varying the same factors. Figure 12.3 shows the simulated ESR spectra of nitroxide, NN, and IN radicals, modulated on the basis of anisotropic rotational diffusion around the principal x , y , and z axes of the g tensor, the principal y -axis of the g tensor, and (again) the principal y -axis of the g tensor, respectively, using the Chili program within the slow-motion regime with respect to the ESR time scale. The associated τ_R values are based on the typical spectra in rotational diffusion of organic radicals in 1D nanochannels and are 6×10^{-9} s for spectra (a)–(c), 3×10^{-8} s for (d), and 9×10^{-9} s for (e) [27, 41, 44, 52]. See Sects. 12.4 and 12.5 about the examples of experimental and simulated ESR spectra of various organic radicals in CLPOT and TPP nanochannel.

12.2.4 Van Vleck's Formula for Rigid Spin Lattices

Sections 12.2.4 and 12.2.5 describe the theoretical background associated with determining the line widths and profiles of broader isotropic ESR spectra in 1D

organic radical chains constructed in 1D nanochannels. This discussion is helpful with regard to clarifying the inter-spin interactions within 1D 4-X-TEMPO chains in 1D nanochannels.

The line profiles of isotropic ESR spectra reflect the type and magnitude of inter-spin dipolar and/or exchange interactions in the specimen, as well as the inter-spin distances between electron spins and other factors. In the absence of exchange interactions (i.e., considering only dipolar interactions in the spin system), the average second moment, M_2 , of the rigid spin lattice can be estimated using Van Vleck's formula [39, 44, 59]

$$M_2 = \Delta\omega^2 = \frac{3}{5}\gamma^4\hbar^4S(S+1)\sum_k\frac{1}{r_k} \quad (12.8)$$

where γ , S , and r_k are the electron gyromagnetic ratio, the electron spin quantum number, and the distance between two spins. In this case, the ESR profile becomes a Gaussian function. Generally, the peak-to-peak line width ΔB_{pp} is equal to $2\sqrt{M_2}$ and the FWHM, $\Delta B_{1/2}$ is equal to $2.36\sqrt{M_2}$ [59]. Under the condition of the existence of only dipolar interaction in the spin system, the peak-to-peak line width is described by B_{pp}^D in this chapter. It should be noted that the experimental value for ΔB_{pp} may be much narrower than the value estimated using Eq. (12.8), as a result of exchange or motional averaging. Therefore, it is necessary to estimate the inter-spin distance in the system as accurately as possible.

In our previous work regarding [(TPP)₂-(TEMPO)_{1,0}] (**1a/2a**) and [CLPOT-(4-X-TEMPO)] (**1b/2a-d**), the electron spins on the NO groups of 4-X-TEMPO molecules in TPP or CLPOT nanochannels were found to interact with those of other 4-X-TEMPO molecules in the same or adjacent channels [39]. These interactions are, respectively, defined as "intra-chain" or "inter-chain" inter-spin interaction. In **1a/2a** and **1b/2a-d**, a single 4-X-TEMPO molecule (i.e., one unpaired electron) was determined to be accommodated in a TPP or CLPOT unit cell formed by two molecules. The electron spins of 4-X-TEMPO molecules in the nanochannels were assumed to be located at the center of gravity of the molecules, so as to simplify computation by averaging the uniaxial rotational diffusion of 4-X-TEMPO molecules around the rotational axis (commonly considered to be parallel to the nanochannel axis). In this case, the nearest neighbor intra-channel or inter-chain inter-spin distance, respectively, corresponds to the cell parameters, such as $c = 1.2$ nm or $a = 0.98$ nm in the case of the TPP frameworks of **1a/2a** [39] and $c = 0.688$ nm or $a = 1.51$ nm in the CLPOT frameworks of **1b/2a** [44]. Therefore, it is convenient to consider **1a/2a** as a spin system having a sixfold symmetric spin lattice with 1.2 nm intra-channel and 0.98 nm inter-channel inter-spin distances. The structures of **1b/2a-d** were interpreted in a similar manner.

However, subsequent studies showed that these assumptions are valid only near room temperature. In this temperature range, 4-X-TEMPO molecules in the TPP or CLPOT nanochannels undergo rotational diffusion in the fast-motion region on the ESR time scale ($\tau_R < 10^{-9}$ s, where τ_R is the correlation time for the rotational

diffusion of 4-X-TEMPO molecules; see Sect. 12.2.3.4). As an example, in **1a/2a** below 112 K, the rotational diffusion of TEMPO molecules in TPP nanochannels is thought to cease, such that the nitroxide groups of TEMPO molecules at different sites are likely disordered [39]. Nevertheless, the relative error associated with the estimations of M_2 using the simple model described in reference [39] and the more precise model taking into account the disorder of nitroxide groups noted above is at most 10%. Similar results are obtained for **1b/2a-d** [44]. Therefore, the simple model based on reference [39], in which the positions of the electron spins of 4-X-TEMPO molecules in the 1D nanochannels are assumed to coincide with the centers of gravity of 4-X-TEMPO molecules, is thought to be suitable as a means of reducing the computational demands when determining M_2 .

12.2.5 Dietz's Method for Determination of ESR Line Profiles and Inter-spin Interactions

The ESR line profile [39, 44, 59, 69] is determined by the Fourier transform of the time-dependent relaxation function of transverse magnetization, $\varphi(t)$ expressed as:

$$\varphi(t) = \exp \left[-M_2 \int_0^t (t - \tau) \Psi(\tau) d\tau \right] \quad (12.9)$$

where $\Psi(\tau)$ is the normalized transverse magnetization correlation function of the local field at the spin. In the absence of an exchange interaction between two electron spins, $\varphi(t)$ can be described by a Gaussian function, resulting in a Gaussian resonance line. In the case of a spin system with 3D interactions due to exchange, or with motional averaging, $\Psi(\tau)$ rapidly decays to zero, leading to an exponential function for $\varphi(t)$ and a Lorentzian resonance line. If $\Psi(\tau)$ decays according to the diffusion equation at the long time region ($\tau_e \ll \tau$, where τ_e is approximately equal to $1/\omega_e$ where ω_e is the spin fluctuation frequency), $\varphi(t)$ for 1D spin diffusion process can be represented as $\exp[-(\Gamma t)^{3/2}]$ where Γ is a constant. This suggests the presence of exchange interactions between neighboring spins in the 1D system. Since the effect of exchange narrowing becomes weaker than that of 3D exchange interactions between spins in this scenario, the ESR line profile will be intermediate between Lorentzian and Gaussian.

The dimensionality of 1D OIC-OR exchange interactions can be assessed by examining the temperature dependency of the ESR line profile using a Dietz's plot [69], which depicts the inverse of the ESR line profile. In such plots, $I(B_0)/I(B)$ is plotted against $[(B-B_0)/(\Delta B_{1/2}/2)]^2$ (see Figs. 12.14 and 12.15 in Sect. 12.6) where $I(B)$ is the intensity of the ESR resonance line in an external magnetic field B , B_0 is the magnetic field on resonance, and $\Delta B_{1/2}$ is the FWHM of the resonance line (meaning that the term $\Delta B_{1/2}/2$ included in the horizontal axis parameter is the half width at half maximum of the resonance line). Figures 12.14 and 12.15 in Sect. 12.6 present one such plot. The magenta one demonstrates a Gaussian function having

the power index of $\varphi(t)$ is population to $-t^2$. The green line in this same figure depicts a Lorentzian function in which $\varphi(t)$ showing an exponential manner, while the cyan curve is for the case intermediate between Gaussian and Lorentzian observed in 1D spin diffusion systems.

12.3 Experimental Procedure

12.3.1 Sample Preparation and Notation

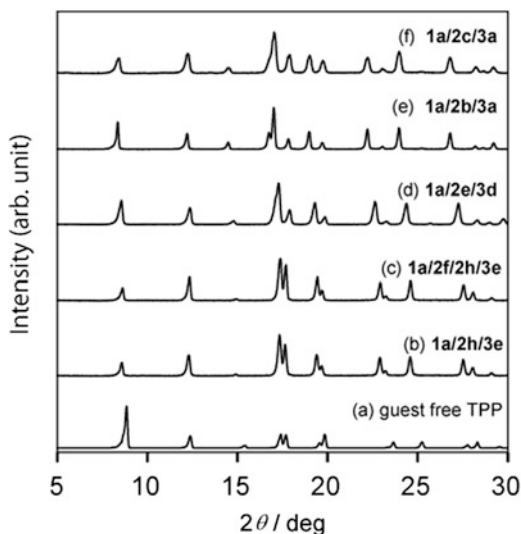
For the investigation of the molecular orientations and dynamics of organic radicals in 1D nanochannels, the appropriate spacer molecules for the dilution of radicals included in TPP or CLPOT nanochannels were selected. The resulting material comprised needle-like crystallites and was colorless. For the construction of 1D organic radical chains in 1D nanochannels, a solution of the radical species was prepared having an excess concentration and without the spacer species. The resulting material comprised needle-like crystallites and was pale orange or pale pink. The reader is referred to several papers that provide detailed preparation process of 1D OIC-OR [27, 39, 41, 44, 52]. Most of 1D OIC-ORs prepared in this way were stable for at least a year in air.

In this chapter, the notation [(A)₂-(B)_x/(C)_y] is used for 1D OIC-OR. For example, when TPP, 4-X-TEMPO, and 4-R-TEMP are used to as host, guest, and spacer, respectively, the notation becomes [(TPP)₂-(4-X-TEMPO)_x/(4-R-TEMP)_y]. *x* and *y* denote the numbers of incorporated units per two host molecules. Throughout the text, the sample names may also be abbreviated simply as “**1a/B/C**” or “**1b/C**.” Note that the host to guest ratio notation for each sample has been abbreviated for the sake of simplifying the figure or in the case of focusing only the component materials of 1D OIC-OR (e.g., the notation of [(TPP)-(4-X-TEMPO)/(4-R-TEMP)] is used for [(TPP)₂-(4-X-TEMPO)_x/(4-R-TEMP)_y]).

12.3.2 Sample Characterization

The structures of TPP and CLPOT nanochannels are known to be maintained even after the inclusion of guest radicals. In addition, the space group and cell parameters of CLPOT crystals are similar following inclusion. However, following inclusion, the cell parameters and pore diameters of TPP crystal can be expanded according to the molecular cross section of the guest radical. Figure 12.4 presents the room temperature powder X-ray diffraction (XRD) patterns obtained for guest-free TPP, [(TPP)₂-(PhIN)_{0.002}/(N-PhMI)_{1.0}] (**1a/2h/3e**) [44], [(TPP)₂-(PhNN)_x/(PhIN)_y/(N-PhMI)_{1.0}] (*x* ≈ 5 × 10⁻⁴ and *y* ≈ 2 × 10⁻⁴; **1a/2f/2h/3e**) [44], [(TPP)₂-(DTBN)_x/(pivalone)_{1.1}] (*x* ≈ 4 × 10⁻⁴; **1a/2e/3d**) [41], [(TPP)₂-(TEMPONE)_{0.021}/(TEMP)_{1.1}] (**1a/2b/3a**) [41], and [(TPP)₂-(TEMPOL)_{0.004}/(TEMP)_{1.2}] (**1a/2c/3a**) [43]. In Figs. 12.4a–f, the reflection patterns

Fig. 12.4 Powder XRD patterns of (a) guest-free TPP, (b) [(TPP)₂-(PhIN)_{0.002}/(N-PhMI)_{1.0}] (1a/2h/3e) [44], (c) [(TPP)₂-(PhNN)_x/(PhIN)_y/(N-PhMI)_{1.0}] ($x \approx 5 \times 10^{-4}$ and $y \approx 2 \times 10^{-4}$; 1a/2f/2h/3e) [44], (d) [(TPP)₂-(DTBN)_x/(pivalone)_{1.1}] ($x \approx 4 \times 10^{-4}$; 1a/2e/3d) [41], (e) [(TPP)₂-(TEMPONE)_{0.021}/(TEMP)_{1.1}] (1a/2b/3a) [41], and (f) [(TPP)₂-(TEMPOL)_{0.004}/(TEMP)_{1.2}] (1a/2c/3a) [43] at room temperature



at small degree values are shifted to the lower degree side as the molecular cross section of the guest radical is increased, demonstrating the expansion of the pore diameters of the TPP nanochannels. The reader is directed to various literature publications that discuss estimation of the cell parameters in various ICs [41–44]. In contrast, the reflection patterns in CLPOT ICs incorporating organic radicals are independent of the presence of guest radicals [51, 52], possibly because of the larger pore diameter of these nanochannels. The inclusion amounts and the composition ratios of guest radicals and spacers in the nanochannels in TPP or CLPOT ICs can be determined according to the ESR spin concentrations, the elemental analysis (EA) results, and the desorption amounts indicated by thermogravimetric analysis – differential thermal analysis (TG-DTA) [27]. The spin concentration in each IC can be obtained from ESR spectra. The composition ratio of guest molecules to host materials or of guest radicals to spacers can be determined from EA data. Finally, in each IC, the possibility of the inclusion of guest molecules in the nanochannels or the adsorption of such species on the host crystal surfaces is given by TG-DTA results. There are several literature reports that provide detailed descriptions of the composition ratios in ICs [39–44, 51–53].

12.4 ESR Analysis of Molecular Orientations and Dynamics of Organic Radicals in CLPOT Nanochannels

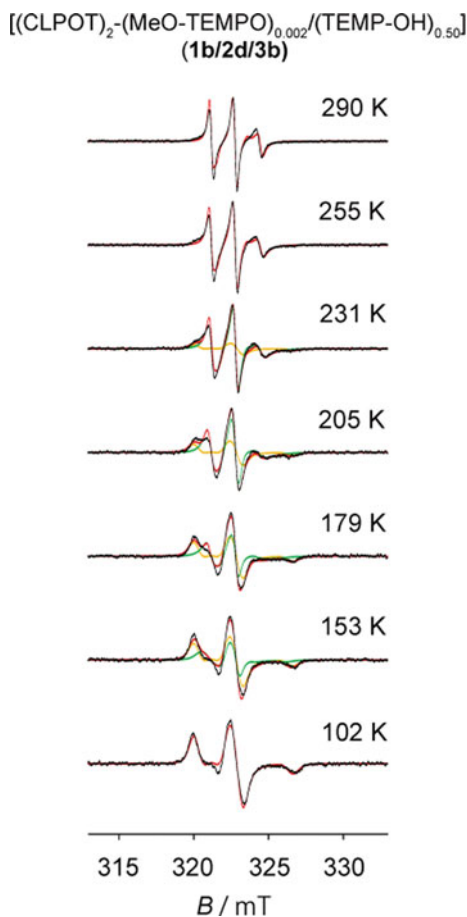
As reported in our previous publication [27, 51–53] various organic radicals can be included in CLPOT nanochannels. If these guest organic radicals are adequately dispersed by spacer molecules with sizes similar to those of the guest, or by

vacancies between guest radicals, the molecular orientations and dynamics of the guest radicals can be examined using ESR spectroscopy and spectral simulations. The reader is referred to several papers that provide detailed experimental conditions for ESR analyses [27, 39, 41, 44, 52].

CLPOT nanochannel can include many organic radicals due to its large pore diameters (1.1–1.2 nm in the guest-free state) and minimal polarity. In this section, the ESR spectra of 4-X-TEMPO and 4-XPNN are presented, and the process of spectral reproduction is explained. The results are used to elucidate the molecular orientations and dynamics of guest radicals in the CLPOT nanochannels.

Figure 12.5 shows temperature-dependent ESR spectra acquired from $[(\text{CLPOT})_2-(\text{MeO-TEMPO})_{0.002}/(\text{TEMP-OH})_{0.50}]$ (**1b/2d/3b**) between 102 and 290 K [52]. All these spectra have been normalized to have the same maximum peak-to-peak height. Green, yellow, and red lines indicate the rotational diffusion, rigid-limit components of the MeO-TEMPO radicals in the CLPOT nanochannels

Fig. 12.5 Temperature dependence of the ESR spectra acquired from $[(\text{CLPOT})_2-(\text{MeO-TEMPO})_{0.002}/(\text{TEMP-OH})_{0.50}]$ (**1b/2d/3b**) [52]. All these spectra have been normalized to have the same maximum peak-to-peak height. A rigid powder pattern of the isolated MeO-TEMPO radical below 102 K, a superposition of a rigid-limit powder pattern (yellow), a slow anisotropic rotational diffusion component (green; $10^{-9} \text{ s} < \tau_R < 10^{-6} \text{ s}$) in the range of 153–231 K, and a slow anisotropic rotational diffusion component in the range of 255–290 K. (Reprinted with permission from *Magn. Reson. Chem.* **2016**, *54*, 641. Copyright 2018 Wiley.)



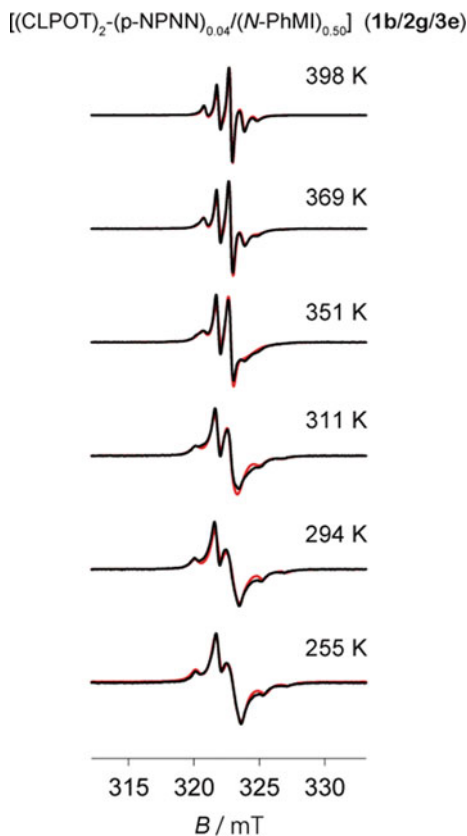
as generated using the EasySpin program (see Sect. 12.2.3.2) [46, 47], and their superpositions, respectively. The spin concentration for each sample remained unchanged after the temperature-dependent ESR analyses. The ESR spectra below 102 K for **1b/2d/3b** were reproduced on the basis of a rigid-limit powder pattern showing an isolated nitroxide radical (see Sect. 12.2.3.3). The ESR spectra in this figure do not include fine structure peaks originating from the formation of radical clusters [37] in the CLPOT nanochannels. Therefore, at these low temperatures, the MeO-TEMPO radicals in **1b/2d/3b** were evidently adequately isolated and did not exhibit molecular motion on the ESR time scale (i.e., $\tau_R > 10^{-6}$ s). The experimental **1b/2d/3b** ESR spectra in Fig. 12.5 were generated using the *g* and *A* tensor components in Table 12.3. The Gaussian and Lorentzian line widths of these components were 0.56 and 0.24 mT, respectively. The values for the *g* and *A* tensors for **1b/2d/3b** were estimated using the Pepper program within EasySpin program (see Sect. 12.2.3.2 and Table 12.3) and were consistent with values reported previously for different 4-X-TEMPO compounds under other conditions (see Table 12.3).

The ESR spectra for **1b/2d/3b** shown in Fig. 12.5 evidently change with increasing temperature, in accordance with a model for the anisotropic rotational diffusion of nitroxide radicals within the slow-motion region relative to the ESR time scale ($10^{-9} < \tau_R < 10^{-6}$) (see Sect. 12.2.3.4). Over the range of 255–290 K, these spectra can be simulated using the Chili program within EasySpin. The ESR spectra at 290 K were reproduced by assuming rotational diffusion around an axis tilted by $(\theta, \varphi) = (65^\circ, 42^\circ)$ relative to the principal *g* tensor system, with Gaussian and Lorentzian line width components of 0.011 and 0.19 mT, respectively, and τ_R equal to 6.5×10^{-9} s. The spectra for temperatures above 255 K were also accurately simulated based on the anisotropic rotational diffusion model around the same rotation axis applied in the case of the 290 K data. The results obtained for CLPOT nanochannel incorporated 4-X-TEMPO with a spacer other than TEMP gave similar (θ, φ) values [51, 52]. These results demonstrate that the molecular orientations of guest 4-X-TEMPO molecules in CLPOT nanochannels are independent of the specific 4-position substituent group or spacer molecules.

In contrast, the **1b/2d/3b** spectra obtained in the intermediate-temperature range (153–231 K) were reproduced using a superposition of rigid and anisotropic rotational diffusion (i.e., mobile) components (yellow and green, respectively, in Fig. 12.5). The mobile components in this temperature range were based on the rotational diffusion model previously discussed, around the same rotational axis as had been applied when working with the 290 K data, but with longer τ_R values (Fig. 12.5). With increasing temperature, the peak intensities of the rigid components were reduced, whereas those of the mobile components were increased due to the wide distribution of τ_R resulting from the local inhomogeneity of the host structure and/or guest packing in these ICs.

The procedure applied for **1b/2d/3b** are also available for 4-XPNN radicals, of which molecular orientations and dynamics in nanospaces were not adequately known before [66]. Figure 12.6 presents the temperature-dependent ESR spectra for $[(\text{CLPOT})_2-(p\text{-NPNN})_{0.04}/(N\text{-PhMI})_{0.5}]$ (**1b/2g/3e**) over the temperature range from 255 to 398 K [27]. The red lines in Fig. 12.6 indicate simulated **1b/2g/3e**

Fig. 12.6 Temperature dependence of the ESR spectra for $[(\text{CLPOT})_2-(p\text{-NPNN})_{0.04}/(N\text{-PhMI})_{0.50}]$ (**1b/2g/3e**). Each red line indicates the spectrum simulated using the EasySpin program package [46, 47]. The ESR spectra for **1b/2g/3e** below 255 K were well-reproduced on the basis of the rigid-limit powder pattern of $p\text{-NPNN}$ radicals. The spectra for **1b/2g/3e** above 294 K were reproduced an anisotropic rotation diffusion model for $p\text{-NPNN}$ in CLPOT nanochannels. (Reprinted with permission from *J. Phys Chem. A* **2014**, *118*, 4907. Copyright 2018 American Chemical Society.)



spectra generated using EasySpin program. The **1b/2g/3e** spectra were unchanged below 255 K within experimental error and were well-reproduced based on the rigid-limit powder pattern of an isolated NN radical shown in Fig. 12.2b (see Sect. 12.2.3.3). Therefore, it appears that the $p\text{-NPNN}$ radicals included in the CLPOT nanochannels of **1b/2g/3e** were adequately isolated by spacers and the molecular motion was frozen with respect to the ESR time scale (i.e., $\tau_R > 10^{-6}$ s). The $p\text{-NPNN}$ spectra at 255 K were simulated using the g and A tensor components in Table 12.3, and the respective Gaussian and Lorentzian line width components were 0.06 and 0.88 mT for **1b/2g/3e**. The values of the g and A tensors for **1b/2g/3e** estimated using the EasySpin program were consistent with the results reported by D'Anna *et al* [66]. Similar results were also obtained for PhNN in CLPOT nanochannels [27]. In the case of isolated NN radicals in CLPOT nanochannels, a change in the ESR spectra from the rigid-limit data was observed above 255 K [51, 52], while temperature was found to affect the ESR spectra of 4-X-TEMPO radicals in CLPOT even above 100 K (see above). The difference in initiation temperature of a change in the ESR spectra is attributed to the fact that the NN radicals have larger molecular size and interaction with the wall of CLPOT than the TEMPO derivatives.

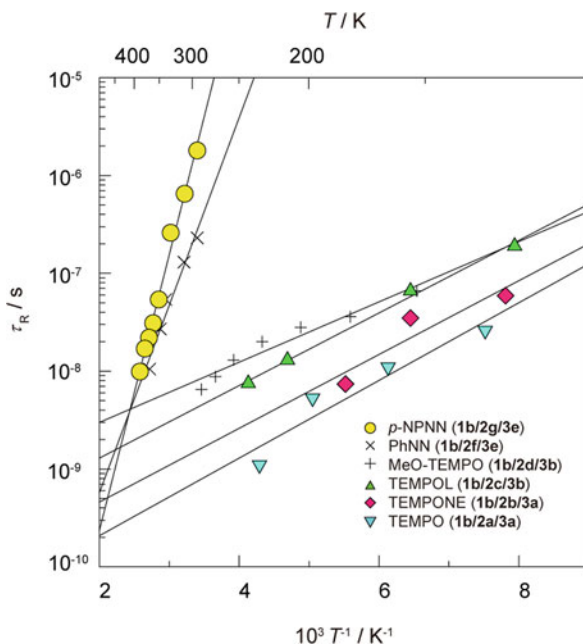
Figure 12.6 shows continuous changes in the ESR spectra with increases in temperature. In the vicinity of 351 K, the **1b/2g/3e** spectra exhibit two narrower peaks between lines 2 and 3 in Fig. 12.2b (see Sect. 12.2.3.4) [27, 66]. In addition, a modulated quintet associated with the two ^{14}N atoms for which $I = 1$ in the NN group appears above 369 K for *p*-NPNN. The temperature-dependent ESR spectra of **1b/2g/3e** were reproducible based on a model for assumption anisotropic rotational diffusion of isolated *p*-NPNN molecules in CLPOT nanochannels within the slow-motion regime with respect to the ESR time scale ($10^{-9} \text{ s} < \tau_{\text{R}} < 10^{-6} \text{ s}$) over the entire temperature range in Fig. 12.6. The **1b/2g/3e** spectra at 398 K were obtained by assuming rotational diffusion around the axis tilted by $(\theta, \phi) = (74^\circ, 90^\circ)$ relative to the principal system of the *g* tensor, with Gaussian and Lorentzian line width components and τ_{R} of 0.11 and 0.30 mT and $1.0 \times 10^{-8} \text{ s}$, respectively. The ESR spectra were also well-reproduced at other temperatures using the anisotropic rotational diffusion model around the same rotation axis.

The rotational axes in **1b/2g/3e** are approximately parallel to the principal *y*-axis of the *g* tensor ($\theta = \phi = 90^\circ$). For this reason, *p*-NPNN molecules are expected to be included in the CLPOT nanochannels with the longest molecular axis parallel to the channel axis, assuming that the rotational axis is parallel to the channel axis. The (θ, ϕ) parameters for the rotational axis relative to the principal axis for *p*-NPNN are larger than those for PhNN ($(\theta, \phi) = (68^\circ, 78^\circ)$). This difference is likely the result of the ratio of the molecular lengths of the NN radicals relative to the pore diameter for the CLPOT nanochannels (0.9 nm for PhNN, 1.1 nm for *p*-NPNN, and 1.1–1.3 nm for CLPOT).

The effects of temperature on τ_{R} for various [(CLPOT)-(4-X-TEMPO)] or [(CLPOT)-(4-XPNN)] are shown in Fig. 12.7 [27, 51, 52]. The rotational activation energy, E_{a} , for 4-X-TEMPO rotation in each [(CLPOT)-(4-X-TEMPO)] was estimated to be in the range of 6–8 kJ mol $^{-1}$, using the τ_{R} values plotted in this figure. Thus, all [(CLPOT)-(4-X-TEMPO)] have similar E_{a} values, and this value is independent of the size or type of the substituent group or the total inclusion amount. This independence may result from the relatively large pore diameter of the CLPOT nanochannels relative to the sizes of the radical molecules. However, the τ_{R} values for [(CLPOT)-(4-X-TEMPO)] are an order of magnitude greater than the value for **1a/2a/3a**. This result suggests that the pore diameter of the nanochannels is an important factor determining τ_{R} .

The high-temperature side in Fig. 12.7 demonstrates the temperature dependence of τ_{R} for [(CLPOT)-(PhNN)/(*N*-PhMI)] (diagonal crosses) and [(CLPOT)-(*p*-NPNN)/(*N*-PhMI)] (yellow circles) [27]. The τ_{R} values for PhNN or *p*-NPNN rotations in [(CLPOT)-(PhNN)/(*N*-PhMI)] and [(CLPOT)-(*p*-NPNN)/(*N*-PhMI)] are much longer than those for 4-X-TEMPO radicals in these nanochannels at the same temperature. As an example, τ_{R} for TEMPO or TEMPOL is on the order of 10^{-9} s at room temperature [51], whereas τ_{R} for the NN radical was approximately 10^{-7} s [27]. The E_{a} values for PhNN and *p*-NPNN rotations in [(CLPOT)-(PhNN)/(*N*-PhMI)] and [(CLPOT)-(*p*-NPNN)/(*N*-PhMI)] were estimated to be 37 and 54 kJ mol $^{-1}$, respectively, using the τ_{R} values in the range of 293–400 K in Fig. 12.7 [27]. These values are several times larger than those for 4-X-TEMPO [51,

Fig. 12.7 Temperature dependence of the rotation diffusion correlation time τ_R for the isolated organic radicals in the CLPOT nanochannels such as *p*-NPNN (**1b/2g/3e**) [27], PhNN (**1b/2f/3e**) [27], MeO-TEMPO (**1b/2d/3b**) [52], TEMPOL (**1b/2c/3b**) [51], TEMPONE (**1b/2b/3a**) [52], and TEMPO (**1b/2a/3a**) [51]



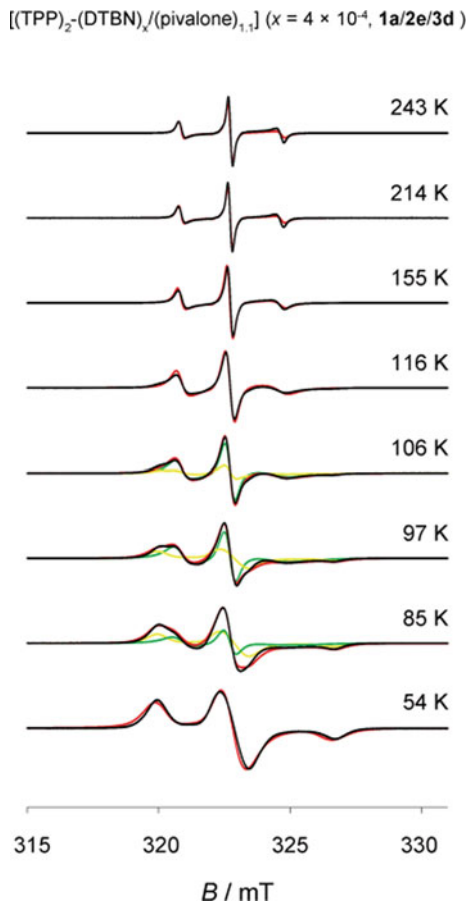
[52]. This difference may be due to the molecular size and weight of the NN radicals (which are larger and heavier than 4-X-TEMPO) as well as stronger interactions between NN radicals and the surrounding host or other guest molecules. Such interactions result from the delocalization of spin density on the nitronyl nitroxide group of the NN radical for which, as opposed to 4-X-TEMPO, the spin density is wrapped internally.

12.5 ESR Analysis of Isolated Organic Radical in 1D TPP Nanochannels

The pore diameters of TPP nanochannels are adjustable over the range of 0.45–0.9 nm to the size of guest molecules [14, 28, 29]. The guest radicals in TPP nanochannels undergo uniaxial rotational diffusion motion in the relatively smaller space than the case of CLPOT. Under such conditions, the molecular orientations and dynamics of guest molecules in these nanospaces are dependent on the molecular size [70]. Although the inclusion of guest radicals is limited due to the smaller pore diameter of TPP nanochannels and/or the minimal polarity of TPP molecules, systematic investigations are possible for several 4-X-TEMPO compounds and for simple NN and IN radicals.

Figure 12.8 provides the temperature-dependent ESR spectra acquired for $[(\text{TPP})_2\text{-(DTBN)}_x\text{-(pivalone)}_{1,1}]$ ($x = 4 \times 10^{-4}$; **1a/2e/3d**) from 54 to 243 K

Fig. 12.8 Experimental and reproduced ESR spectra of $[(\text{TPP})_2\text{-(DTBN)}_x\text{/(pivalone)}_{1,1}]$ ($x = 4 \times 10^{-4}$; **1a/2e/3d**) [41]. Green, yellow, and red lines of **1a/2e/3d** indicate the rotational diffusion and rigid-limit components of the DTBN radicals in the TPP nanochannels reproduced using the EasySpin program package and their superposition. (Reprinted with permission from *J. Phys Chem. A* **2013**, *117*, 2093. Copyright 2018 American Chemical Society.)



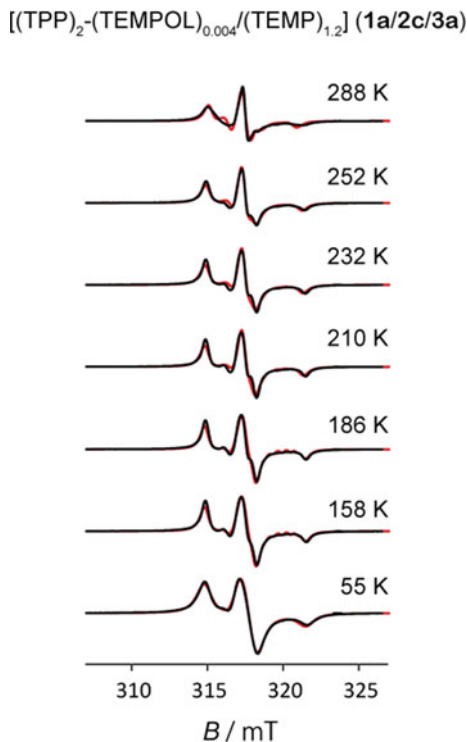
[41]. Here, green, yellow, and red lines indicate the rotational diffusion, rigid-limit components of the DTBN radicals in the TPP nanochannels as reproduced using EasySpin program [46, 47], and their superposition. At 54 K, a typical pattern of a rigid-limit nitroxide radical, similar to that in Fig. 12.5 is observed (see Sects. 12.2.3.3 and 12.4). This result demonstrates that the DTBN molecules were adequately isolated in the TPP nanochannels. The narrowed ESR spectra of **1a/2e/3d** at 214 K provide evidence for the uniaxial rotational diffusion of DTBN in the TPP nanochannels within the slow-motion regime with respect to the ESR time scale around the y-axis of the g tensor of the DTBN molecule. The g and A tensors of the DTBN molecules in the TPP nanochannels were determined, as summarized in Table 12.3, from the 54 K spectrum according to the standard procedure (see Sects. 12.2.3.1, 12.2.3.2, and 12.2.3.3). The calculated g and A tensors are consistent with those of DTBN molecules confined in a tetramethyl-1,3-cyclobutanedione (TMCB) matrix within experimental error [41]. In this simulation, the Gaussian and Lorentzian components of the line width were 0.64 and 0.65 mT, respectively.

The **1a/2e/3d** spectra at 214 K shown in Fig. 12.8 were accurately simulated based on rotation around the axis defined by $(\theta, \phi) = (86^\circ, 89^\circ)$ in the principal axis system of the \mathbf{g} and \mathbf{A} tensors in Table 12.3. These simulations assumed that R_{\parallel}/R_{\perp} had a value of approximately 1000, τ_R was approximately 7.5×10^{-9} s and that the line widths of the Gaussian and Lorentzian components were 0.08 and 0.15 mT, respectively (see Sect. 12.2.3.4). The direction of the rotational axis was estimated to be almost parallel to the principal y -axis ($\theta = 90^\circ, \phi = 90^\circ$). That is, the nitroxide groups of uniaxially rotating DTBN molecules confined in TPP nanochannels are considered to be almost perpendicular to the rotational axis, which in turn can be assumed to be parallel to the channel axis. When TEMPO or TEMPONE are dispersed in TPP nanochannels, both the temperature dependency of the ESR spectra and the molecular orientations of the guest radicals in the TPP nanochannels are similar [40, 41]. In the range of 85–106 K, the ESR spectra were reproduced by the superposition of a rigid component and an axially rotational diffusion component, though it was not reproduced by simple rigid or axially rotational diffusion components. These results provide evidence for the coexistence of low- and high-temperature phases, in which the molecular motion of the guest molecules is frozen out and unfrozen, respectively.

When TEMPOL is included as guest radical in TPP nanochannel, molecular orientations and dynamics were quite different from DTBN and other 4-X-TEMPO. Figure 12.9 shows the variable-temperature experimental and simulated ESR spectra for a powdered sample of $[(\text{TPP})_2-(\text{TEMPOL})_{0.004}/(\text{TEMP})_{1.2}]$ (**1a/2c/3a**) [43]. At 55 K, the ESR spectrum of **1a/2c/3a** demonstrates a rigid-limit for the nitroxide radical that is similar to those of other radicals in the TPP and CLPOT nanochannels (see Figs. 12.5 and 12.8 and Sect. 12.2.3.3). In addition, the principal components of the \mathbf{g} and \mathbf{A} tensors in this case are comparable to those of other nitroxide radicals (see Table 12.3). However, the spectra of **1a/2c/3a** in the higher temperature region (e.g., at 288 K in Fig. 12.9) are quite different from those in Figs. 12.5 or 12.8. According to the spectral simulation, the rotational axis of the TEMPOL molecules in the TPP nanochannels are tilted by $(\theta, \phi) = (19^\circ, 66^\circ)$ in the principal axis system of the \mathbf{g} and \mathbf{A} tensors. These values are close to the principal z -axis of the \mathbf{g} tensor (corresponding to $\theta = 0^\circ$ and an arbitrary ϕ ; see Sect. 12.2.3.4). Thus, it appears that the molecular orientations of guest radicals in TPP nanochannels can be adjusted by the proper selection of guest radicals and spacer molecules, or the co-inclusion of other radicals.

In addition, a rare example of the inclusion of IN or NN radicals in TPP nanochannels has been demonstrated. Figure 12.10 presents the temperature-dependent ESR spectra for $[(\text{TPP})_2-(\text{PhIN})_{0.002}/(\text{N-PhMI})_{1.0}]$ (**1a/2h/3e**) [44]. Here, green, yellow, and red lines indicate the rotational diffusion and rigid-limit components of PhIN in **1a/2h/3e** as reproduced using EasySpin program and their superposition. The spectra acquired at less than 165 K were well-reproduced based on a rigid-limit powder pattern for isolated PhIN (see Sect. 12.2.3.3) [68]. The spectrum for **1a/2h/3e** at 56 K shown in Fig. 12.10 was simulated using the \mathbf{g} and \mathbf{A} tensor components in Table 12.3, and the respective Gaussian and Lorentzian line width components were 0.31 and 0.30 mT. The values of the \mathbf{g}

Fig. 12.9 Temperature dependence of the experimental (black) and reproduced (red) ESR spectra of the powder sample of $[(\text{TPP})_2-(\text{TEMPOL})_{0.004}/(\text{TEMP})_{1.2}]$ (**1a/2c/3a**) in the temperature range of 55–288 K [43]. (Reprinted with permission from *Chem. Lett* **2015**, *44*, 893. Copyright 2018 Chemical Society of Japan.)

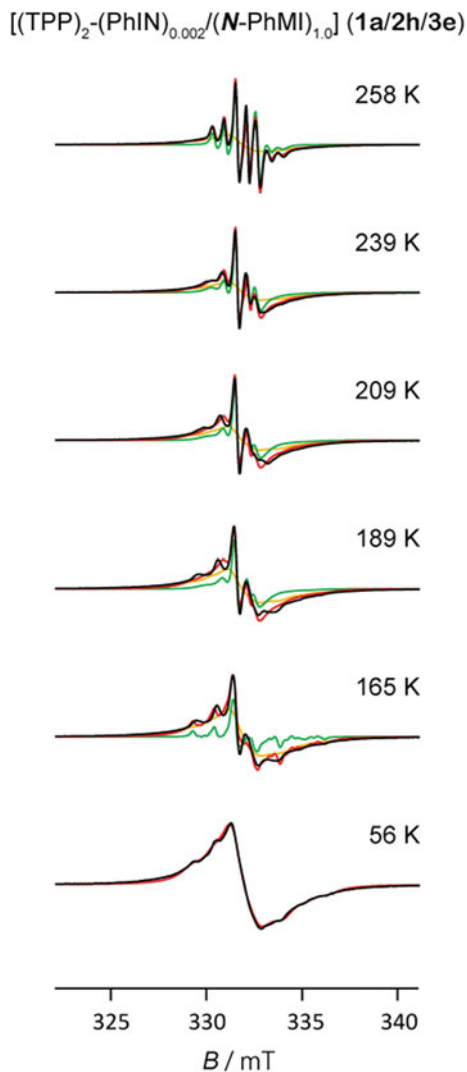


and A tensors for **1a/2h/3e** estimated using EasySpin program were consistent with the previous results obtained for PhIN dispersed in glassy toluene (see Table 12.3) [68]. Therefore, in **1a/2h/3e**, the PhIN radicals may be considered to be adequately isolated in the TPP nanochannels as a result of the use of spacers and/or located on the surfaces of the TPP crystals, and the molecular motion is frozen on the ESR time scale (i.e., $\tau_R > 10^{-6}$ s).

The spectra of **1a/2h/3e** above 165 K depicted in Fig. 12.10 were not generated using a single anisotropic rotational diffusion component but by the superposition of anisotropic rotational diffusion and rigid-limit components. From 258 K to room temperature, the rotational diffusion and rigid-limit components were temperature-independent within experimental error. The anisotropic rotational diffusion component of **1a/2h/3e** in the temperature range from 165 to 258 K was reproduced as a septet associated with two ^{14}N atoms (both $I = 1$, but with different hyperfine coupling constants) in the IN group of PhIN modulated by molecular motion in the slow regime with respect to the ESR time scale. These results suggest that some PhIN radicals may be included in the TPP nanochannels, but that additional PhIN radicals may be on the surfaces of the TPP crystals.

In the case of PhIN in diluted solutions or in nanospaces within the fast-motion regime on the ESR time scale, seven major hyperfine splitting lines associated with the inequivalent nitrogen atoms of IN with $A_{1zz}^{\text{IN}} \sim 2A_{2zz}^{\text{IN}}$ are observed, with

Fig. 12.10 Temperature-dependent ESR spectra for $[(\text{TPP})_2-(\text{PhIN})_{0.002}/(N\text{-PhMI})_{1.0}]$ (**1a/2h/3e**) [44]. Green, yellow, and red lines indicate rotational diffusion and rigid-limit components of PhIN in **1a/2h/3e** reproduced using the EasySpin program package [46, 47] and their superposition. (Reprinted with permission from *J. Phys Chem. A* **2018**, *122*, 5493. Copyright 2018 American Chemical Society.)



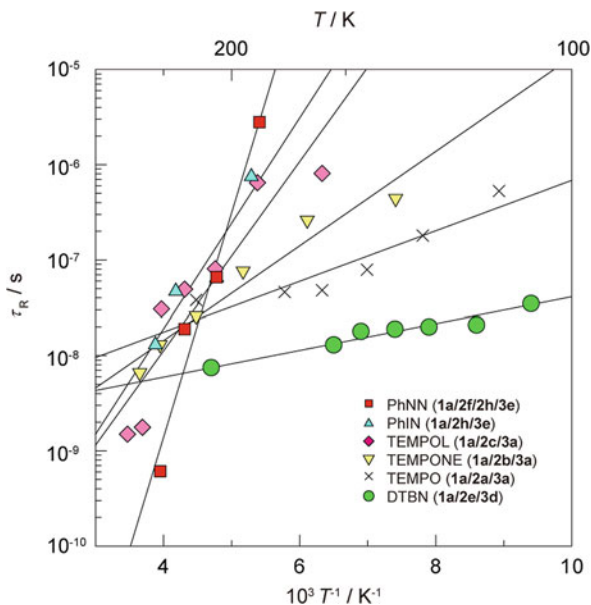
an intensity ratio of 1:1:2:1:2:1:1. However, with the molecular motion around the principal y -axis of the g tensor in the slow regime on the ESR time scale, the ESR spectra of PhIN radicals are modulated as shown in Fig. 12.3e (see Sect. 12.2.3.4 and reference [44]). When a low-temperature rigid-limit component is superposed, the spectral reproduction at 258 K is improved, as shown in Fig. 12.10. In fact, the modulated septet of the ESR spectrum of **1a/2h/3e** at 258 K is simulated reasonably well assuming that the anisotropic rotational diffusion around the axis is tilted by $(\theta, \phi) = (90^\circ, 73^\circ)$ relative to the principal axis system of the g tensor and parallel to the principal y -axis, with Gaussian and Lorentzian line width components and

τ_R of 0.17 and 0.036 mT and 1.3×10^{-8} s, respectively. These results show that the rotational axis is also approximately parallel to the molecular long axis of the PhIN molecules (i.e., the molecular long axis is parallel to the channel axis of the TPP nanochannels, if it is assumed that the rotational axis is parallel to the channel axis). Every ESR spectrum collected over the range from 165 to 239 K was also reproduced using this same approach. Based on the spectral reproduction process, it is evident that at least some PhIN radicals are included in the TPP nanochannels, although other PhIN radicals in **1a/2h/3e** may be adsorbed on the surfaces of the TPP crystals.

PhNN radicals can also be included in TPP nanochannels [44]. However, as some PhNN is reduced to PhIN during the synthetic process, [(TPP)₂-(PhNN)_x/(PhIN)_y/(N-PhMI)_{1.0}] ($x \approx 5 \times 10^{-4}$ and $y \approx 2 \times 10^{-4}$, **1a/2f/2h/3e**) is produced. According to the ESR results, PhNN radicals included in the TPP nanochannels undergo anisotropic rotational diffusion around a rotational axis tilted by $(\theta, \phi) = (90^\circ, 89^\circ)$ relative to the principal axis system of the g tensor above 253 K.

Figure 12.11 summarizes the effect of temperature on τ_R for isolated organic radicals in TPP nanochannels, including PhNN (**1a/2f/3e**), PhIN (**1a/2h/3e**), TEMPOL (**1a/2c/3a**), TEMPONE (**1a/2b/3a**), TEMPO (**1a/2a/3a**), and DTBN (**1a/2e/3d**) [40, 41, 43, 44]. The τ_R of each radical can be approximately determined from the rotational Stokes-Einstein relationship, assuming that the material behaves as an anisotropic liquid (see Sect. 12.2.3.4) [45]. The E_a values of several nitroxide radicals (such as DTBN, TEMPO, and TEMPONE) increase as the substituent groups become larger (with values 3, 5, and 10 kJ mol⁻¹) [40, 41]. In addition,

Fig. 12.11 Temperature dependence of the rotational diffusion correlation time τ_R , for the isolated organic radicals in the TPP nanochannels such as DTBN (**1a/2e/3a**), TEMPO (**1a/2a/3a**), TEMPONE (**1a/2b/3a**), TEMPOL (**1a/2c/3a**), PhIN (**1a/2h/3e**), and PhNN (**1a/2f/3e**) [40, 41, 43, 44]



the E_a values for PhIN and PhNN rotations in TPP nanochannel (19 and 45 kJ mol⁻¹) are much greater than those for such nitroxide radicals [44]. These results indicate that the τ_R values in TPP nanochannels are determined by the moment of inertia for guest radicals. Alternatively, these data may result from the strong interactions of PhIN or PhNN with the surrounding host walls formed by the phenyl rings of TPP molecules. Interactions may also occur with neighboring spacers in the TPP nanochannels as a result of the delocalization of the spin density on the iminonitroxide groups of PhIN radicals or the nitronylnitroxide group of NN radicals, in contrast to the behavior of TEMPO (in which the spin density is wrapped inside). However, the E_a value for PhIN rotation is smaller than that for 4-hydroxy-TEMPO (TEMPOL) in TPP nanochannels (26 kJ mol⁻¹) [43]. The E_a for TEMPOL rotation has been reported to be much larger than those for other TEMPO derivatives due to the different molecular orientation of TEMPOL in TPP nanochannels, as shown above (see Fig. 12.9). In the case of PhIN and TEMPOL in TPP nanochannels, the NO groups are approximately perpendicular to the nanochannel axis and also close to the nanochannels walls formed by the phenyl rings of TPP molecules [14, 28, 29], assuming that the rotational axis is parallel to the channel axis. The larger E_a for TEMPOL rotation in TPP nanochannel may be caused by the additional interaction between the OH groups (rather than the NO groups) of TEMPOL and the π -clouds on the phenyl rings of the TPP wall. This is as opposed to hydrogen bridging of the OH groups of TEMPOL with the oxygen atoms or the lone pairs of the nitrogen atoms of the TPP structure.

The molecular orientations of NN radicals in TPP or CLPOT nanochannels is as same each other as discussed in Sects. 12.4 and 12.5, that is, the molecular long axis is parallel to the channel axis. In addition, the E_a value for PhNN rotation in TPP nanochannel is larger than that for PhNN rotation in CLPOT nanochannel (37 kJ mol⁻¹, see Fig. 12.7). This result may be due to the smaller pore diameter of TPP nanochannels compared to those in CLPOT. The E_a value for PhNN rotation in TPP nanochannel is smaller than that for *p*-NPNN in CLPOT nanochannels (54 kJ mol⁻¹, see Fig. 12.7). This outcome is attributed to the smaller moment of inertia for PhNN compared to that for *p*-NPNN. In addition, PhNN rotation gives larger E_a value than PhIN rotation. It may be attributable to the difference in the steric hindrances of NN and IN groups, or to the stronger intermolecular interactions of PhNN with neighboring spacer molecules.

12.6 1D 4-X-TEMPO Chains Constructed in CLPOT and TPP Nanochannels

The ESR measurements for organic radicals in 1D nanochannels dispersed by spacer molecules were conducted in Sects. 12.4 and 12.5. In such systems, dipolar and/or exchange interaction between radicals can be ignored due to the longer intermolecular distance, although 1D molecular chains are formed (see Fig. 12.12a).

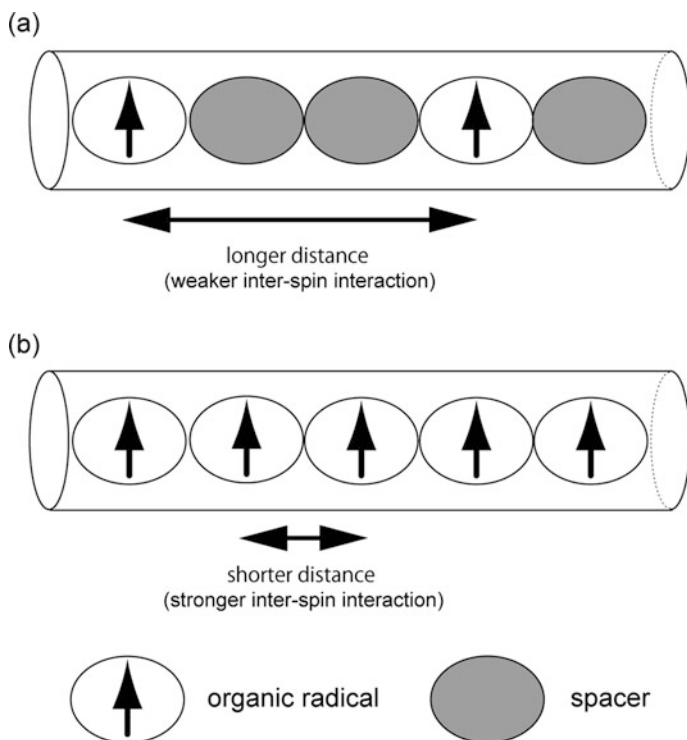


Fig. 12.12 Images of intermolecular distance and inter-spin interaction between radicals included in 1D nanochannel described in Sects. 12.4 and 12.5. (a) Isolated radical dispersed by spacer in CLPOT or TPP nanochannel described in Sects. 12.4 and 12.5. (b) 1D molecular chain of organic radicals in CLPOT and TPP nanochannel described in this section

In this section, the inter-spin interaction of 1D molecular chains of 4-X-TEMPO constructed in CLPOT and TPP nanochannels (without any spacers; see Fig. 12.12b) is discussed herein, based on the ESR spectra of [(CLPOT)-(4-X-TEMPO)] and [(TPP)-(4-X-TEMPO)]. In particular, the dimensionality and magnitude of these interactions are examined in terms of the molecular dynamics of guest radicals in the CLPOT and TPP nanochannels. Approximately, the inter-spin interactions of organic radical chain in CLPOT nanochannel are independent of the molecular orientations and dynamics of guest radicals, whereas those in TPP nanochannel are affected by the molecular dynamics of guest radicals described in Sects. 12.4 and 12.5.

Figure 12.13 summarizes the effect of temperature on the peak-to-peak line width ΔB_{pp} values (see Sect. 12.2.4) associated with the ESR spectra of [(TPP)₂-(TEMPO)_{1,0}] (**1a/2a**; diagonal crosses), [(CLPOT)₂-(TEMPO)_{1,0}] (**1b/2a**; yellow triangles), [(CLPOT)₂-(TEMPOL)_{1,0}] (**1a/2c**; empty circles), [(CLPOT)₂-(TEMPONE)_{1,1}] (**1a/2b**; magenta diamonds), and [(CLPOT)₂-(MeO-TEMPOL)_{0,91}] (**1a/2d**; cyan squares) over the temperature range from 4.2 to

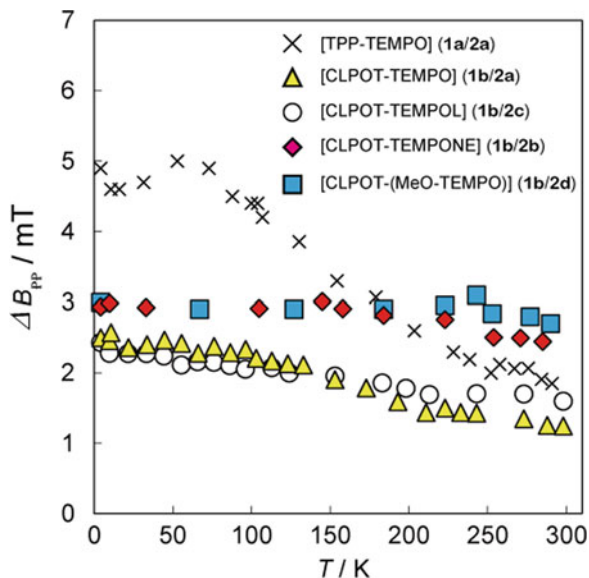


Fig. 12.13 Temperature dependency of the ESR spectra of the ΔB_{pp} of isotropic ESR spectra of [(TPP)₂-(TEMPO)_{1,0}] (diagonal crosses; **1a/2a**), [(CLPOT)₂-(TEMPO)_{1,0}] (yellow triangles; **1b/2a**), [(CLPOT)₂-(TEMPOL)_{1,0}] (empty circles; **1a/2c**), [(CLPOT)₂-(TEMPONE)_{1,1}] (magenta diamonds; **1a/2b**), and [(CLPOT)₂-(MeO-TEMPOL)_{0,91}] (**1a/2d**; cyan squares) in the temperature range from 4.2 to 300 K [41, 53]. Note that the composition ratio of host to guest in each sample in the figure was abbreviated in the figure for simplification. (Reprinted with permission from *Bull. Chem. Soc. Jpn.* **2018**, *91*, 375. Copyright 2018 Chemical Society of Japan.)

300 K [53]. Note that the composition ratio of host to guest in each sample has been abbreviated in this figure for simplification. Isolated 4-X-TEMPO radicals in the 1D TPP or CLPOT nanochannels generate anisotropic ESR signals, as discussed in Sects. 12.4 and 12.5. However, in the case of spin systems having spin concentrations greater than those for isolated radicals (as shown in this section), the ESR spectra appear isotropic because the line width of the 4-X-TEMPO absorption line becomes broader than the hyperfine coupling of the nitroxide. This occurs due to significant dipole interactions and minimal exchange narrowing.

The effect of temperature on the ΔB_{pp} values of [(TPP)₂-(TEMPO)_{1,0}] (**1a/2a**) are summarized as follows. These effects are related to the molecular motions of TEMPO radicals in TPP nanochannels [39, 40, 53]. The essentially steady value of ΔB_{pp} of approximately 4.8 mT below 100 K reflects the termination of the molecular motion of TEMPO radicals in the TPP nanochannels. In addition, the gradual decrease of ΔB_{pp} with increasing temperature in the range of 100–253 K reflects the rotational diffusion of these radicals in the nanochannels within the slow-motion regime on the ESR time scale (10^{-9} s < τ_R < 10^{-6} s). The almost constant value ($\Delta B_{pp} = 1.8$ mT) above 253 K indicates rotational diffusion within the fast-motion regime on the ESR time scale (τ_R < 10^{-9} s). The variations in ΔB_{pp} values

between the highest and lowest temperatures are close to 3.6 mT. Above 100 K, the experimental ΔB_{pp} values for **1a/2a** are smaller than the estimated dipolar peak-to-peak line width (ΔB_{pp}^D ; see Sect. 12.2.4) based on Van Vleck's formula for a rigid spin lattice (Eq. (12.8) in Sect. 12.2.4), indicating exchange narrowing due to the temperature dependency of the ESR line profile (see below and Fig. 12.15).

On the other hand, the effect of temperature on the ΔB_{pp} values of **1b/2a-d** is evidently more gradual than that for **1a/2a**, although there is a slight decrease with increases in temperature. The magnitude of the ΔB_{pp} values for **1b/2a-d** was at most 2–3 mT even at low temperature, and the variation with increasing in temperature was less than 1.4 mT, even at 300 K. The ΔB_{pp} value is also somewhat larger when the 4-position substituent group on the TEMPO molecule is bulkier. Because the crystal structure of the CLPOT nanochannels and the quantity of guest radicals per unit cell in each [CLPOT-(4-X-TEMPO)] are similar to the values for **1a/2a** (see Sect. 12.3.2), the dipolar peak-to-peak line width (ΔB_{pp}^D , see Sect. 12.2.4) for **1b/2a-d** was estimated assuming a hexagonal rigid spin lattice formed by positioning the electron spin in the CLPOT nanochannels at the center of gravity of the TEMPO molecule [39, 53] (see Sect. 12.2.4). Using this model, the ΔB_{pp}^D value for **1b/2a-d** was estimated to be 11.2 or 11.3 mT. A significantly larger ΔB_{pp}^D was evidently obtained from the shorter *c* (*i.e.*, shorter intra-channel inter-spin distance of 0.7 nm) [50] of **1b/2a-d** as compared to **1a/2a**. These results indicate the narrowing of ESR line width of **1b/2a-d** due to molecular motion or exchange interaction.

The ESR line profiles were determined according to the theory described in Sect. 12.2.5. Figure 12.14 shows the effect of temperature on the line profiles of [(TPP)₂-(TEMPO)_{1,0}] (**1a/2a**; diagonal crosses) and of [CLPOT-(4-X-TEMPO)], such as [(CLPOT)₂-(TEMPO)_{1,0}] (**1b/2a**, yellow triangles), [(CLPOT)₂-(TEMPOL)_{1,0}] (**1a/2c**, empty circles), [(CLPOT)₂-(TEMPONE)_{1,1}] (**1a/2b**, magenta diamonds), and [(CLPOT)₂-(MeO-TEMPOL)_{0,91}] (**1a/2d**, cyan squares) according to Dietz's method (see Sect. 12.2.5) at 4.2, 155 K, and 290 K [39, 53]. Note that the host to guest ratio notation for each sample in Fig. 12.14 has been abbreviated for the sake of simplifying the figure.

In the case of **1b/2a-d**, the molecular motions of guest radicals in CLPOT nanochannels are temperature-dependent, as shown in Sect. 12.4, with a rigid-limit under about 120 K. With increases in temperature (above 200–240 K), the rotational diffusion motion originally in the slow-motion regime on the ESR time scale changed such that τ_R moved into the fast-motion region of the ESR time scale. In addition, τ_R of **1b/2a-d** was shorter than the value for TEMPO in the TPP nanochannels in the same temperature range (see Figs. 12.7 and 12.11) [41, 43, 52]. The **1b/2a-d** line profiles were almost independent of temperature, as seen in Fig. 12.14a–c, indicating different results compared to those obtained for **1a/2a** (see below and Fig. 12.15). These data suggest that the molecular motions and/or substituent groups of guest radicals in the CLPOT nanochannels are not correlated with the inter-spin interactions of **1b/2a-d**. Therefore, the narrower ESR line width for **1b/2a-d** may be considered to originate not from motional narrowing but rather than 3D exchange interactions. This finding demonstrates that 3D exchange

Fig. 12.14 Dietz's plot of isotropic ESR spectra of [(TPP)₂-(TEMPO)_{1.0}] (**1a/2a**; diagonal crosses) and the [CLPOT-(4-X-TEMPO)] (**1b/2a**, yellow triangles; **1b/2c** empty circles; **1b/2b**, magenta diamonds; and **1b/2d**, cyan squares) according to Dietz's method at (a) 4.2, (b) 155 K, and (c) 290 K [41, 53]. Note that the composition ratio of host to guest of each sample in the figure was abbreviated in the figure for simplification. (Reprinted with permission from *Bull. Chem. Soc. Jpn.* **2018**, *91*, 375. Copyright 2018 Chemical Society of Japan.)

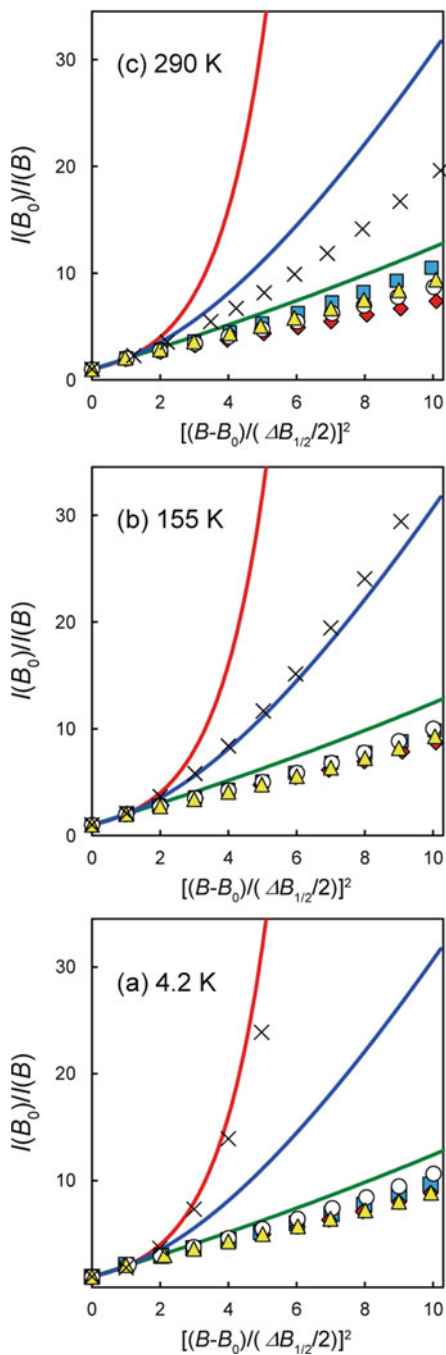
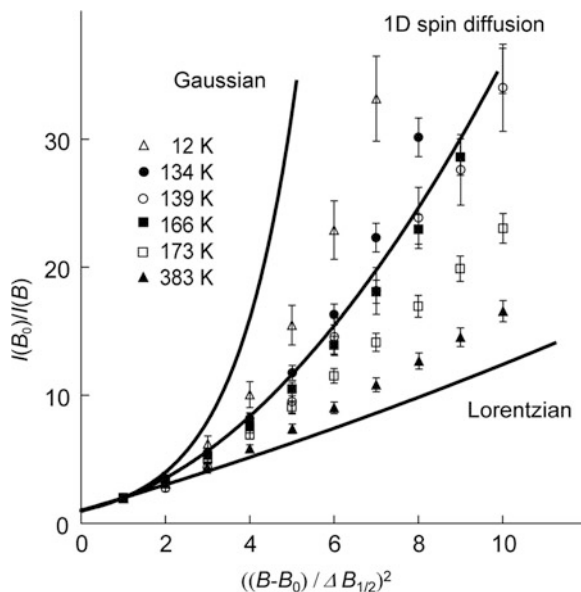


Fig. 12.15 Temperature dependency of line shape of [(TPP)₂-(TEMPO)_{1.0}] (**1a/2a**) in 12–383 K using Dietz' method. (Reprinted with permission from *Bull. Chem. Soc. Jpn.* **2007**, *80*, 711. Copyright 2018 Chemical Society of Japan.)



interactions can be observed even in 1D OIC-OR by selecting the optimal host and/or guest compounds. The 3D exchange interactions of organic radical chains in [CLPOT-(4-X-TEMPO)] may result from the formation of an imperfect 1D electron spin array due to the disordered orientation of the nitroxide groups of guest 4-X-TEMPO molecules in the CLPOT nanochannels, which have larger pore diameters than those in TPP.

Figure 12.15 shows the effect of temperature on the ESR line profiles of [(TPP)₂-(TEMPO)_{1.0}] (**1a/2a**), as determined using Dietz's method (see Sect. 12.2.5). In the temperature range from 12 to 139 K, approximately corresponding to the rigid-limit of TEMPO in TPP nanochannels, the line shape exhibits characteristics intermediate between those expected from the pure Gaussian and 1D spin diffusion models. Therefore, the 1D spin diffusion mechanism occurs even at fairly low temperature, where TEMPO rotation is frozen in TPP nanochannel. Over the range of 139–166 K, corresponding to τ_R values of approximately 10^{-7} s for TEMPO in TPP nanochannels, the **1a/2a** line shape is in good agreement with that expected from the pseudo-1D-spin diffusion model. This result obviously indicates that exchange narrowing explains the narrowing seen in Fig. 12.13. At temperatures greater than 166 K (corresponding to $\tau_R < 10^{-8}$ s), the resonance peak become more Lorentzian with increases in temperature, although a pure Lorentzian line shape never appears, even at 383 K. This increase in the Lorentzian character suggests that anisotropic exchange interactions occur between interchain spins. These interchain interactions cut off $\Psi(\tau)$ after a characteristic time (see Sect. 12.2.5). The line shape at 383 K roughly reflects the ratio of intrachain exchange interactions, J_{intra} , to interchain exchange interactions, J_{inter} , giving a $J_{\text{inter}}/J_{\text{intra}}$ ratio in the range of 10^{-2} – 10^{-3} [71,

72]. The average molecular orientation of TEMPO in TPP nanochannel by rotational diffusion provides homogeneous interaction between unpaired electrons in adjacent TEMPOs. This scenario produces a large exchange integral, thus increasing the efficiency of exchange narrowing. The exchange integral in this system may be calculated based on the wavefunction perturbed by molecular motion of guest radicals in TPP nanochannel. For these reasons, **1a/2a** is a remarkable material, as the dimensionality of the exchange interactions changes from 1D to 3D with increasing temperature (compare this result to that in CLPOT above).

In other [TPP-(4-X-TEMPO)], a few interesting experimental results are known. [(TPP)₂-(DTBN)_{1,3}] (**1a/2e**) exhibits a similar effect of temperature on ΔB_{pp} to **1a/2a** [42]. However, the ΔB_{pp}^D value for **1a/2e** estimated from Eq. (12.8) (approximately 9 mT) is significantly larger than that for **1a/2a**. Therefore, the line width of **1a/2e** is thought to be much narrower than that for **1a/2a**. In addition, the ESR line profiles for [(TPP)₂-(DTBN)_{1,3}] (**1a/2e**) are also temperature-dependent, but 1D spin diffusion behavior is observed around room temperature [42], while [TPP-TEMPONE] (**1a/2b**) shows temperature-dependent anisotropic exchange interaction even in the vicinity of 4.2 K. Thus, [TPP-(4-X-TEMPO)] is unique among the various 1D OIC-OR.

12.7 Concluding Remarks and Outlook

In CLPOT and TPP nanochannels, incorporated organic radicals form 1D organic radical chain. To examine the 1D or 3D exchange interactions in 1D organic radical chain, molecular dynamics of organic radicals in the nanochannels were assessed by experimental and theoretical ESR analyses.

It was found that molecular dynamics of 4-X-TEMPO radical in CLPOT nanochannel is independent of the substituent groups of the guest radicals and/or the type of spacer. From ESR adsorption line profiles and the molecular dynamics of 4-X-TEMPO radicals in CLPOT nanochannels, it was found that [CLPOT-(4-X-TEMPO)] exhibits temperature-independent 3D exchange interactions. The existence of 3D exchange interaction in [CLPOT-(4-X-TEMPO)] may be the first step to express magnetic phase transition in 1D OIC-OR.

On the other hand, [TPP-(4-X-TEMPO)] exhibited temperature-dependent anisotropic exchange interaction. It may be correlated with temperature dependency on molecular dynamics of guest radical in TPP nanochannel with a small pore diameter. These different exchange interaction in CLPOT and TPP nanochannels will be a key to design and develop a new organic magnet.

The molecular dynamics of 4-XPNN and PhIN radicals in CLPOT or TPP nanochannels was clarified using ESR analyses. These results may be available to the development of a new ESR spin probe technique using NN or IN radicals for the clarification of the structure of nanospaces in polymer, liquid crystal, and membrane. It is expected that spin system based on 4-XPNN or PhIN radicals will be formed in 1D OIC-OR by the increase of the guest inclusion amount.

The relationship between exchange interactions of organic radical chain and molecular dynamics should be further elucidated in order to design and develop innovative organic magnet. This work is underway.

Acknowledgments These works were partially supported by the Strategic Research Base Development program for Private Universities of the Ministry of Education, Culture, Sports, Science and Technology of Japan (MEXT), 2009–2013. These works were also partially supported by the Common Research Funding by Showa University, 2017–2018. The authors wish to thank Professor T. Asaji of Nihon University for assistance with the ESR analyses, Professor T. Hashimoto of Nihon University for assistance with the TG-DTA measurements, Prof. S. Stoll of the University of Washington for assistance with the EasySpin calculations, and the Organic Elemental Analysis Research Center, Kyoto University, for performing the elemental analyses.

References

1. Z. Rinkevicius, B. Frecus, N.A. Murugan, O. Vahtras, J. Kongsted, H. Ågren, Encapsulation influence on EPR parameters of spin-labels: 2,2,6,6-tetramethyl-4-methoxypiperidine-1-oxyl in cucurbit[8]uril. *J Chem Theory Comput* **8**, 257 (2012)
2. S.M. Neville, G.J. Halder, K.W. Chapman, M.B. Duriska, B. Moubaraki, K.S. Murray, C.J. Kepert, Guest tunable structure and spin crossover properties in a nanoporous coordination framework material. *J Am Chem Soc* **131**, 12106 (2009)
3. G.J. Halder, C.J. Kepert, B. Moubaraki, K.S. Murray, J.D. Cashion, Guest-dependent spin crossover in a nanoporous molecular framework material. *Science* **298**, 1762 (2002)
4. D. Tanaka, S. Kitagawa, Template effects in porous coordination polymers. *Chem Mater* **20**, 922 (2008)
5. M. David, T. Kishi, M. Kishaku, H. Nakanishi, H. Kasai, Carbon nanoarch encapsulating Fe nanowire on Ni(111). *Jpn J Appl Phys* **45**, 2869 (2006)
6. R. Kulasekharan, N. Jayaraj, M. Porel, R. Choudhury, A.K. Sundaresan, A. Parthasarathy, M.F. Ottaviani, S. Jockusch, N.J. Turro, V. Ramamurthy, Guest rotations within a capsuleplex probed by NMR and EPR techniques. *Langmuir* **26**, 6943 (2010)
7. N. Jayaraj, M. Porel, M.F. Ottaviani, M.V.S.N. Maddipatla, A. Modeli, J.P. Da Silva, B.R. Bhogala, B. Captain, S. Jockusch, N.J. Turro, V. Ramamurthy, Self aggregation of supramolecules of nitroxides@cucurbit[8]uril revealed by EPR spectra. *Langmuir* **25**, 13820 (2009)
8. D. Fujita, Y. Ueda, S. Sato, N. Mizuno, T. Kumasaka, M. Fujita, Self-assembly of tetravalent Goldberg polyhedra from 144 small components. *Nature* **540**, 563 (2016)
9. V.I. Nikolayenko, L.J. Barbour, A. Arauzo, J. Campo, J.M. Rawson, D.A. Haynes, Inclusion of a dithiadiazolyl radical in a seemingly non-porous solid. *Chem Commun*, 11310 (2017)
10. Q.F. Sun, J. Iwasa, D. Ogawa, Y. Ishido, S. Sato, T. Ozeki, Y. Sei, K. Yamaguchi, M. Fujita, Self-assembled M₂₄L₄₈ polyhedra and their sharp structural switch upon subtle ligand variation. *Science* **328**, 1144 (2010)
11. R. Kitaura, K. Seki, G. Akiyama, S. Kitagawa, Porous coordination-polymer crystals with gated channels specific for supercritical gases. *Angew Chem Int Ed* **42**, 428 (2003)
12. G. Couderc, J. Hulliger, Channel forming organic crystals: guest alignment and properties. *Chem Soc Rev* **39**, 1545 (2010)
13. R. Kitaura, S. Kitagawa, Y. Kubota, T.C. Kobayashi, K. Kindo, Y. Mita, A. Matsuo, M. Kobayashi, H.-C. Chang, T.C. Ozawa, M. Suzuki, M. Sakata, M. Takata, Formation of a one-dimensional array of oxygen in a microporous metal-organic solid. *Science* **298**, 2358 (2002)
14. H.R. Allcock, Cyclophosphazene clathrates-exploring the adjustable tunnel. *Acc Chem Res* **11**, 81 (1978)

15. M. Fanina, G. di Silvestro, P. Sozzani, Perhydrotriphenylene: D_3 symmetric host, in *Comprehensive supramolecular chemistry*, ed. by D. D. MacNicol, F. Toda, R. Bishop, vol. 6, (Pergamon, Oxford, 1996), pp. 371–419
16. R.T. Morrison, R.N. Boyd, *Organic chemistry*, 6th edn. (Prentice-Hall, Inc, 1992)
17. B. Ye, M.L. Trudeau, D.M. Antonelli, Observation of a double maximum in the dependence of conductivity on oxidation state in potassium fulleride nanowires supported by a mesoporous niobium oxide host lattice. *Adv Mater* **13**, 561 (2001)
18. F. Marlow, M. Wübbenhorst, J. Caro, Pyroelectric effects on molecular sieve crystals loaded with dipole molecules. *J Phys Chem* **98**, 12315 (1994)
19. B. Zhou, A. Kobayashi, H. Kobayashi, Dielectric properties of one-dimensional water clusters confined in the porous crystal, $[\text{Co}_3(2,4\text{-pyde})_2(\mu_3\text{-OH})_2] \cdot 9\text{H}_2\text{O}$ (2,4-pyde: pyridine-2,4-dicarboxylate). *Chem Lett* **42**, 1131 (2013)
20. T. Fukino, H. Joo, Y. Hisada, M. Obana, H. Yamagishi, T. Hikima, M. Takata, N. Fujita, T. Aida, Manipulation of discrete nanostructures by selective modulation of noncovalent forces. *Science* **344**, 499 (2014)
21. A.C. Soegiarto, W. Yan, A.D. Kent, M.D. Ward, Regulating low-dimensional magnetic behavior of organic radicals in crystalline hydrogen-bonded host frameworks. *J Mater Chem* **21**, 2204 (2011)
22. D. Bardelang, M. Giorgi, V. Hornebecq, A. Stepanov, M. Hardy, E. Rizzato, V. Monnier, M.B. Zaman, G. Chan, K. Udachin, Hosting various guests including fullerenes and free radicals in versatile organic paramagnetic bTbk open frameworks. *Cryst Growth Des* **14**, 467 (2014)
23. A.R. Albutia, C. D'Aniello, G. Guerra, D. Gatteschi, M. Mannini, L. Sorace, Ordering magnetic molecules within nanoporous crystalline polymers. *Chem Mater* **21**, 4750 (2009)
24. M. Mon, A. Pascual-Alvarez, T. Grancha, J. Cano, J. Ferrando-Soria, F. Lloret, J. Gascon, J. Pasan, D. Armentano, E. Pardo, Solid-state molecular nanomagnet inclusion into a magnetic metal–organic framework: interplay of the magnetic properties. *Chem Eur J* **22**, 539 (2016)
25. J.X. Huang, C.D. Luo, W.B. Li, Y. Li, Y.S. Zhang, J.H. Zhou, Q. Jiang, Eccentric magnetic microcapsules for orientation-specific and dual stimuli-responsive drug release. *J Mater Chem B* **3**, 4530 (2015)
26. K. Tateishi, M. Negoro, S. Nishida, A. Kagawa, Y. Morita, M. Kitagawa, *Proc Natl Acad Sci U S A* **111**, 7527 (2014)
27. H. Kobayashi, Y. Morinaga, E. Fujimori, T. Asaji, ESR study of molecular orientation and dynamics of nitronyl nitroxide radicals in CLPOT 1D nanochannels. *J Phys Chem A* **118**, 4907 (2014)
28. H.R. Allcock, L.A. Siegel, Phosphonitrilic compounds. III.1 Molecular inclusion compounds of Tris(o-phenylenedioxy)phosphonitrile trimer. *J Am Chem Soc* **86**, 5140 (1964)
29. P. Sozzani, S. Bracco, A. Comotti, L. Ferrenti, R. Simonutti, Methane and carbon dioxide storage in a porous van der Waals Crystal. *Angew Chem Int Ed* **44**, 1816 (2005)
30. T. Meersmann, J.W. Logan, R. Simonutti, S. Caldarelli, A. Comotti, P. Sozzani, L.G. Kaiser, A. Pines, *J Phys Chem A* **104**, 11665 (2000)
31. P. Sozzani, A. Comotti, R. Simonutti, T. Meersmann, J.W. Logan, A. Pines, *Angew Chem Int Ed* **39**, 2695 (2000)
32. H. Kobayashi, T. Ueda, K. Miyakubo, T. Eguchi, *Z Naturforsch* **58a**, 727 (2003)
33. T. Hertzsch, S. Kluge, E. Weber, F. Budde, J. Hulliger, *Adv Mater* **13**, 1864 (2001)
34. C. Gervais, T. Hertzsch, J. Hulliger, Insertion of dipolar molecules in channels of a centrosymmetric organic zeolite: molecular modeling and experimental investigation on diffusion and polarity formation. *J Phys Chem B* **109**, 7961 (2005)
35. T. Hertzsch, F. Budde, E. Weber, J. Hulliger, *Angew Chem Int Ed* **41**, 2281 (2002)
36. H.I. Süß, T. Wuest, A. Sieber, R. Althaus, F. Budde, H.-P. Lüthi, G.D. McManus, J. Rawson, J. Hulliger, *CrystEngComm* **4**, 432 (2002)
37. A. Barbon, A. Zoleo, M. Brustolon, A. Comotti, P. Sozzani, One-dimensional clusters of 16-doxyl-stearate radicals in organic nanochannels as studied by electron paramagnetic resonance (EPR). *Inorg Chim Acta* **361**, 4122 (2008)

38. H. Kobayashi, T. Ueda, K. Miyakubo, J. Toyoda, T. Eguchi, A. Tani, Preparation and characterization of new inclusion compound with 1D molecular arrangement of organic radicals using a one-dimensional organic homogeneous nanochannel template. *J Mater Chem* **15**, 872 (2005)
39. H. Kobayashi, T. Ueda, K. Miyakubo, T. Eguchi, A. Tani, Spin-spin interaction of TEMPO molecular chains formed in an organic one-dimensional nanochannel as studied by electron spin resonance (ESR). *Bull Chem Soc Jpn* **80**, 711 (2007)
40. H. Kobayashi, T. Ueda, K. Miyakubo, T. Eguchi, A. Tani, ESR study of molecular dynamics and orientation of TEMPO included in organic one-dimensional nanochannel. *Phys Chem Chem Phys* **10**, 1263 (2008)
41. H. Kobayashi, K. Takeuchi, T. Asaji, Molecular orientation and dynamics of different sized radicals included in organic 1-D nanochannels. *J Phys Chem A* **117**, 2093 (2013)
42. H. Kobayashi, T. Asaji, A. Tani, Preparation and characterization of new inclusion compounds using stable nitroxide radicals and an organic 1-D nanochannel as a template. *Materials* **3**, 3625 (2010)
43. H. Kobayashi, K. Aoki, T. Asaji, Dynamics of TEMPOL radicals in TPP 1D nanochannels and different molecular orientation from other TEMPO derivatives. *Chem Lett* **44**, 893 (2015)
44. H. Kobayashi, T. Mori, Y. Morinaga, E. Fujimori, K. Akiniwa, F. Iwahori, Electron spin resonance study of molecular orientation and dynamics of phenyl imino and nitronyl nitroxide radicals in organic 1D nanochannels of Tris(*o*-phenylenedioxy)cyclotriphosphazene. *J Phys Chem A* **122**, 5493 (2018)
45. J.H. Freed, *Spin labeling, theory and applications*, ed. by L. J. Berliner (Academic, New York, 1976)
46. S. Stoll, A. Schweiger, EasySpin, a comprehensive software package for spectral simulation and analysis in EPR. *J Magn Reson* **178**, 42 (2006)
47. <http://www.easyspin.org/>: see the manual of Chili (2018–12–07)
48. B. Dzikovski, D. Tipikin, V. Livshits, K. Earle, J. Freed, Multifrequency ESR study of spin-labeled molecules in inclusion compounds with cyclodextrins. *Phys Chem Chem Phys* **11**, 6676 (2009)
49. C. Aliaga, F. Bravo-Moraga, D. Gonzalez-Nilo, S. Márquez, S. Lühr, G. Mena, M.C. Rezende, Location of TEMPO derivatives in micelles: subtle effect of the probe orientation. *Food Chem* **192**, 395 (2016)
50. R.K.R. Jetti, P.K. Thallapally, F. Xue, T.C.W. Mak, A. Nangia, Hexagonal nanoporous host structures based on 2,4,6-tris-4-(halo-phenoxy)-1,3,5-triazines (halo = chloro, bromo). *Tetrahedron* **56**, 6707 (2000)
51. H. Kobayashi, T. Asaji, A. Tani, ESR study of the molecular orientation and dynamics of stable organic radicals included in the 1-D organic nanochannels of 2,4,6-tris-4-(chlorophenoxy)-1,3,5-triazine. *Magn Reson Chem* **50**, 221 (2012)
52. H. Kobayashi, Y. Furuhashi, H. Nakagawa, T. Asaji, ESR study of molecular orientation and dynamics of TEMPO derivatives in CLPOT 1D nanochannels. *Magn Reson Chem* **54**, 641 (2016)
53. H. Kobayashi, H. Takamisawa, Y. Furuhashi, H. Nakagawa, K. Nakatsugawa, K. Takeuchi, Y. Morinaga, Inter-spin interaction of CLPOT inclusion compounds with 1D molecular chains of 4-X-TEMPO radicals in the temperature range of 4.2–300 K. *Bull Chem Soc Jpn* **91**, 375 (2018)
54. M. Bonin, G. Labat, G. Couderc, T.A. Lüthi, K. Reichenbacher, J. Hulliger, H.–B. Bürgi, Novel host-guest structures of 2,4,6-*Tris*(4-Halophenoxy)-1,3,5-Triazines (XPOT): inclusion of C₆₀ and pyridine. *J Chem Crystallogr* **42**, 645 (2012)
55. H.I. Süss, J. Hulliger, Organic channel inclusion compound featuring an open pore size of 12 Å. *Microporous Mesoporous Mater* **78**, 23 (2005)
56. B. Naydenov, C. Spudat, W. Harnleit, H.I. Süss, J. Hulliger, J. Nuss, M. Jansen, Ordered inclusion of endohedral fullerenes N@C₆₀ and P@C₆₀ in a crystalline matrix. *Chem. Phys. Lett* **424**, 327 (2006). S.D. Bruce, J. Higinbotham, I. Marshall, P.H. Beswick, An Analytical Derivation of a Popular Approximation of the Voigt Function for Quantification of NMR Spectra. *J Magn Reson* **142**, 57 (2000)

57. H.M. Levitt, *Spin dynamics*, 2nd edn. (Wiley, 2008)
58. C.P. Slichter, *Principles of magnetic resonance*, 3rd edn. (Springer, Heidelberg, 1996)
59. A. Abragam, *Principles of nuclear magnetism* (Oxford/New York, 1961)
60. G.E. Pake, T.L. Estle, *The physical principle of electron paramagnetic resonance*, 2nd edn. (W. A. Benjamin, Inc., New York, 1973)
61. T.T. Tong, T. Yonezawa, N. Toshima, J.J. van der Klink, ^{195}Pt NMR of polymer-protected Pt/Pd bimetallic catalysts. *J Phys Chem B* **100**, 730 (1996)
62. The Spin Hamiltonian (EasySpin), <http://easyspin.org/easyspin/documentation/hamiltonian.html> (2018–12–07).
63. L.J. Libertini, O.H. Griffith, Orientation dependence of the electron spin resonance spectrum of Di-*n*-butyl nitroxide. *J Chem Phys* **53**, 1359 (1970)
64. B.G. Birrell, S.P. Van, O.H. Griffith, Electron spin resonance of spin labels in organic inclusion crystals. Models for anisotropic motion in biological membranes. *J Am Chem Soc* **95**, 2451 (1973)
65. V.F. Tarasov, I.A. Shkrob, A.D. Trifunac, Spin-polarized nitroxide radicals in organic glasses. *J Phys Chem A* **106**, 4838 (2002)
66. J.A. D'Anna, J.H. Wharton, Electron spin resonance spectra of α -nitronyl nitroxide radicals; solvent effects; nitrogen hyperfine tensor; *g* anisotropy. *J Chem Phys* **53**, 4047 (1970)
67. S.A. Dikanov, V.I. Gulin, Y.D. Tsvetkov, I.A. Grigor'ev, 2 mm Electron paramagnetic resonance studies of the new types of imidazoline nitroxide radicals. *J. Chem. Soc. Faraday Trans.* **86**, 3201 (1990)
68. S.D. Bruce, J. Higinbotham, I. Marshall, P.H. Beswick, An analytical derivation of a popular approximation of the voigt function for quantification of NMR spectra. *J. Magn. Reson.* **142**, 57–63 (2000). <https://doi.org/10.1006/jmre.1999.1911>
69. R.E. Dietz, F.R. Merritt, R. Dingle, D. Hone, B.G. Silbernagel, P.M. Richards, Exchange narrowing in one-dimensional systems. *Phys Rev Lett* **26**, 1186 (1971)
70. J.A. Villaunueva-Garibay, K. Müller, Solid-state ^2H NMR studies of cyclophosphazene inclusion compounds: order and dynamics of the benzene guests. *J Phys Chem B* **108**, 15057 (2004)
71. M.J. Hennessy, C.D. McElwee, P.M. Richards, Effect of interchain coupling on electron-spin resonance in nearly one-dimensional system. *Phys Rev B* **7**, 930 (1973)
72. T.T.P. Cheung, Z.G. Soos, R.E. Dietz, F.R. Merritt, Temperature dependence of exchange narrowing in the one-dimensional antiferromagnet $\text{N}(\text{CH}_3)_4\text{MnCl}_3$. *Phys. Rev B* **17**, 1266 (1978)